SSC-465

MODELING IMPACT OF SEA ICE ON SHIP AND OFFSHORE STRUCTURES

SHIP STRUCTURE COMMITTEE
2012

Ship Structure Committee

RADM P.F. Zukunft
U. S. Coast Guard Assistant Commandant,
Assistant Commandant for Marine Safety, Security
and Stewardship
Co-Chair, Ship Structure Committee

RDML Thomas Eccles
Chief Engineer and Deputy Commander
For Naval Systems Engineering (SEA05)
Co-Chair, Ship Structure Committee

Mr. H. Paul Cojeen
Society of Naval Architects and Marine Engineers

Dr. Roger Basu
Senior Vice President
American Bureau of Shipping

Mr. Christopher McMahon
Director, Office of Ship Construction
Maritime Administration

Mr. Victor Santos Pedro
Director Design, Equipment and Boating Safety,
Marine Safety,
Transport Canada

Mr. Kevin Baetsen
Director of Engineering
Military Sealift Command

Dr. Neil Pegg
Group Leader - Structural Mechanics
Defence Research & Development Canada - Atlantic

Mr. Jeffrey Lantz,
Commercial Regulations and Standards for the
Assistant Commandant for Marine Safety, Security
and Stewardship
Mr. Jeffery Orner
Deputy Assistant Commandant for Engineering and
Logistics

Mr. Edward Godfrey
Director, Structural Integrity and Performance Division

Dr. John Pazik
Director, Ship Systems and Engineering Research
Division

SHIP STRUCTURE SUB-COMMITTEE

AMERICAN BUREAU OF SHIPPING (ABS)

Mr. Craig Bone
Mr. Phil Rynn
Mr. Tom Ingram

DEFENCE RESEARCH & DEVELOPMENT CANADA ATLANTIC

Dr. David Stredulinsky
Mr. John Porter

MARITIME ADMINISTRATION (MARAD)
Mr. Chao Lin
Mr. Richard Sonnenschein

MILITARY SEALIFT COMMAND (MSC)
Mr. Michael W. Touma
Mr. Jitesh Kerai

NAVY/ONR / NAVSEA/ NSWCCD
Mr. David Qualley / Dr. Paul Hess
Mr. Erik Rasmussen / Dr. Roshdy Barsoum
Mr. Nat Nappi, Jr.
Mr. Malcolm Witford

TRANSPORT CANADA
Natasa Kozarski
Luc Tremblay

UNITED STATES COAST GUARD

CAPT John Nadeau
CAPT Paul Roden
Mr. Jaideep Sirkar
Mr. Chris Cleary

SOCIETY OF NAVAL ARCHITECTS AND MARINE ENGINEERS (SNAME)
Mr. Rick Ashcroft
Mr. Dave Helgerson
Mr. Alex Landsburg
Mr. Paul H. Miller

SSC – 465
SR – 1466

NOVEMBER 30, 2011

PREDICTIVE MODELING IMPACT OF ICE ON SHIP AND OFFSHORE STRUCTURES

Increased interest in navigating through polar waters requires a better understanding of potential ship hull damage caused by collisions with polar sea ice. An analysis and comparison of recent predictive method advances in modeling fracture mechanics and the elasto-plastic responses of hull materials and structure to sea ice impacts is crucial to developing a modern modeling framework. Accordingly, this project investigates recently developed numerical methods and evaluates their capabilities and applicability toward evaluating ships structures for adequate residual strength following ice impact damage.

Of the three promising technologies identified, only two are identified as commercially available, the Element Free Galerkin Method (EFGM) and the Extended Finite Element Method (X-FEM). Of those two methods, one is significantly more computationally intensive than the other. Therefore, while all three methods are described theoretically within this study, only X-FEM is explored in detail through actual execution and is compared to typical FEM analysis techniques. Results show the advantage of using the X-FEM for obtaining better resolution of crack propagation through the enriched elements defined by this method; while the Baseline FEM is limited to modeling crack propagation along pre-defined element boundaries. The conclusion provides recommendations regarding the appropriate applicability for using either the EFGM or X-FEM methods.

We thank the authors and Project Technical Committee for their dedication and research toward completing the objectives and tasks detailed throughout this paper and continuing the Ship Structure Committee's mission to enhance the safety of life at sea.

P. F. ZUKUNFT
Rear Admiral, U.S. Coast Guard
Co-Chairman, Ship Structure Committee

T. J. ECCLES
Rear Admiral, U.S. Navy
Co-Chairman, Ship Structure Committee

1. Report No. 465	2. Government Accession No.	3. Recipient's Catalog No. 4002DE

4. Title and Subtitle Predictive Modeling Impact of Ice on Ship and Offshore Structures		5. Report Date 1 June 2011
		6. Performing Organization Code

7. Author(s) Alejandro Bueno	8. Performing Organization Report No. SR-1466

9. Performing Organization Name and Address CSC 1201 M Street SE Suite 400 Washington, DC 20003	10. Work Unit No. (TRAIS)
	11. Contract or Grant No. N00178-04-D-4030 EH02

12. Sponsoring Agency Name and Address COMMANDANT (CG-5212/SSC) ATTN (SHIP STRUCTURE COMMITTEE) US COAST GUARD 2100 2ND ST SW STOP 7126 WASHINGTON DC 20593-7126	13. Type of Report Final Report
	14. Sponsoring Agency Code CG - 5

15. Supplementary Notes
The research completed by the above author for the Ship Structure Committee was reviewed by the Project Technical Committee for satisfactory completion of the objectives outlined in the Statement of Work developed and approved for funding by the Principal Members of the Ship Structure Committee.
Sponsored by the Ship Structure Committee and its member agencies

16. Abstract

Increased interest in navigation through polar waters calls for better understanding of potential ship hull damage from collision with sea ice. Recent advances on numerical methods for modeling fracture mechanics on steel plating offers a means for developing a modeling framework which can be used for study and analysis of such hull damage. The numerical methods that are considered most suitable for this application are selected and studied; the commercial package LS-DYNA is used for developing a modeling framework. Results from this evaluation are presented and discussed.

CONVERSION FACTORS
(Approximate conversions to metric measures)

To convert from	to	Function	Value
LENGTH			
inches	meters	divide	39.3701
inches	millimeters	multiply by	25.4000
feet	meters	divide by	3.2808
VOLUME			
cubic feet	cubic meters	divide by	35.3149
cubic inches	cubic meters	divide by	61,024
SECTION MODULUS			
inches^2 feet^2	centimeters^2 meters^2	multiply by	1.9665
inches^2 feet^2	centimeters^3	multiply by	196.6448
inches^4	centimeters^3	multiply by	16.3871
MOMENT OF INERTIA			
inches^2 feet^2	centimeters^2 meters	divide by	1.6684
inches^2 feet^2	centimeters^4	multiply by	5993.73
inches^4	centimeters^4	multiply by	41.623
FORCE OR MASS			
long tons	tonne	multiply by	1.0160
long tons	kilograms	multiply by	1016.047
pounds	tonnes	divide by	2204.62
pounds	kilograms	divide by	2.2046
pounds	Newtons	multiply by	4.4482
PRESSURE OR STRESS			
pounds/inch^2	Newtons/meter^2 (Pascals)	multiply by	6894.757
kilo pounds/inch^2	mega Newtons/meter^2 (mega Pascals)	multiply by	6.8947
BENDING OR TORQUE			
foot tons	meter tons	divide by	3.2291
foot pounds	kilogram meters	divide by	7.23285
foot pounds	Newton meters	multiply by	1.35582
ENERGY			
foot pounds	Joules	multiply by	1.355826
STRESS INTENSITY			
kilo pound/inch^2 inch$^{1/2}$(ksi$\sqrt{}$in)	mega Newton MNm$^{3/2}$	multiply by	1.0998
J-INTEGRAL			
kilo pound/inch	Joules/mm^2	multiply by	0.1753
kilo pound/inch	kilo Joules/m^2	multiply by	175.3

Table of Contents

Executive Summary

Recent advances on numerical methods for predicting fracture mechanics on elasto-plastic materials are of significant interest for the study of crack initiation and propagation on steel plates.

The task of this project, which is to "investigate the development of a predictive modeling framework for Sea Ice impact on the ship hull structure", required the following activities
- review the applicability of these new advanced methods to the task.
- select the methods for which numerical algorithms have been developed and exist in commercial codes.
- develop a modeling framework that facilitates the evaluation of these methods and the analysis of specific scenarios and ship structures. The main components of this framework are: 1) ice load modeling methodology, 2) pre-processor, 3) FEM software, 4) Post-processor
- Test and verify the functionality of the modeling framework by applying the selected methods.

A comprehensive literature review on the advancements on new methodologies for simulating crack propagation on elasto-plastic and brittle materials yielded three methods that, to date, have received much interest from the community of numerical computation. These methods are: The Trefftz method, the Element Free Galerkin method (EFGM) and the Extended Finite Element method (X-FEM). A commercially available structural analysis software program with the latter two methods implemented and validated was selected: LS-DYNA.

A pre-processor for generating the model definition and scenario conditions in the LS-DYNA input data format was developed. It generates the data inputs required for the classical Finite Element method (FEM), the EFGM and the X_FEM. This pre-processor also facilitates the process of batch execution of runs covering the design space or field of study.

The EFGM requirements for mesh definition of the model exceeded the limitations of the available hardware and number of software licenses; the estimated runtime by the solver for one case was in excess of 58,000 minutes. Consequently, only the X-FEM was tested and compared to the Baseline FEM. The results obtained show the advantage of using the X-FEM for obtaining better resolution of crack propagation through the enriched elements defined by this method; while the Baseline FEM is limited to modeling crack propagation along pre-defined element boundaries.

Results of the study can be used only for comparison of the standard FEM and the X-FEM methods. This relative comparison of the two methods suggests that the former is sufficiently adequate for studies and analyses that do not require high accuracy of the path of propagation of initiated cracks from impact; for cases where accurate prediction of crack propagation is required, the X-FEM is the recommended approach..

As a future step in the development of this predictive modeling framework, it is recommended to perform a thorough validation with reliable experimental data.

7

Introduction

The evaluation of new shipping routes through northern regions that have partially ice covered waters requires new knowledge about the risks of ship hull damage caused by the collision with polar sea ice. It is the purpose of this task to investigate new advanced methodologies for accurate evaluation of the effects on the structural integrity of ship hulls that are subjected to these ice loads.

Theoretical Background

An extensive literature review of studies related to the subject of structural damage, including crack initiation and propagation on elasto-plastic plates, yielded information on several new advanced methods well suited for modeling the impact and damage of sea ice on the hull structure of ships traveling through polar waters. These new methods improve on the standard computational Finite Element Method (FEM) for modeling the propagation of cracks [1-2].

Three promising new methodologies have undergone significant study and further development. These are: the Trefftz method, the Element Free Galerkin Method (EFGM) and the Extended Finite Element Method (X-FEM). The implementation of the latter two methods in commercially available software is relatively recent and limited to few commercial codes. Generally, the approach of these methods is characterized by adding local enrichment to the initial topology in the form of added degrees of freedom. These methods can be broadly classified as:

- Adaptive p-enrichment (polynomial) methods: The Trefftz is the earliest and most studied in its class.
- Meshless methods: The EFGM is the best known and most extensively studied in this class and has been implemented in a limited number of commercial codes.
- Enrichment by localized functions: The X-FEM has made significant advances since its original development in modeling initiation and propagation of discontinuities. X-FEM is the most recent of of the three methods reviewed; it is implemented in a limited number of commercial codes.

Trefftz Method

The Trefftz method, frequently referred as hybrid-Trefftz method, [3-7] uses p-adaptive macro elements featuring higher order polynomial shape functions than the standard FEM. This method shares essential features of the Boundary Element Method (BEM) in that the boundary conditions are implemented locally by a "collocation method". The Trefftz method uses two alternative approximation models for enforcement of inter-element and boundary continuity conditions: a) A Displacement model generates kinematically admissible solutions; boundary tractions are approximated and used to enforce the inter-element displacement continuity condition and the kinematic condition. b) A Stress model generates statically admissible solutions; boundary displacements are approximated and used to enforce the inter-element traction continuity condition and static boundary condition.

Because no commercial software was found to have this method implemented, no further discussion is made on this method.

Element Free Galerkin Method (EFGM)

The EFGM [8-13] requires only a set of nodes and the description of the model's boundaries as input. The most significant advantage over the standard FEM is that it handles large deformations and is mesh-independent.

The EFGM generates shape functions for each node that describe their domain of influence. These shape functions have the following constraints: a) they do not have influence across boundary and/or crack domains; b) they are defined within a region of 'compact support'. Figures 1 and 2 [1, 11] illustrate these shape functions and their domains of influence.
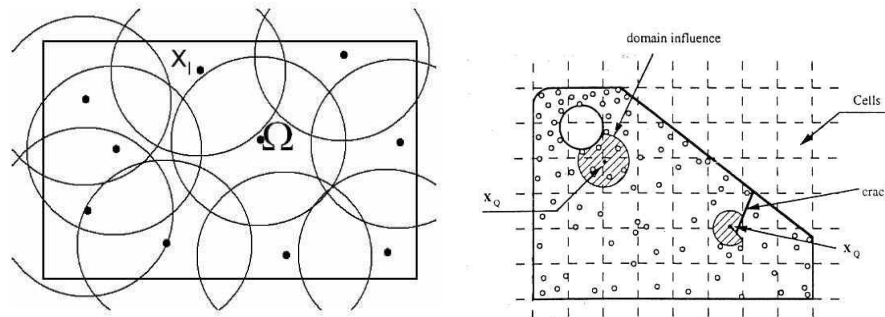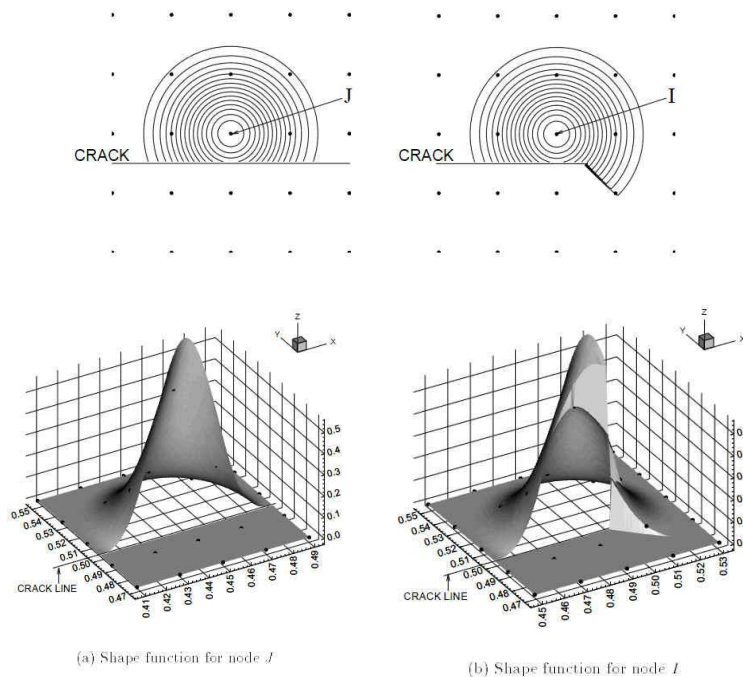

Figure 1 – Nodal shape functions domain of influence

Figure 2 – Nodal shape function

EFGM Formulation:

The EFGM employs a Moving Least Squares interpolant $u^h(\mathbf{x})$ to approximate the function of displacement,

$$u^h(x) = \sum_{j}^{m} p_j(x) \cdot a_j(x) \equiv \mathbf{p}^T(x) \cdot \mathbf{a}(x) \tag{1}$$

where $p_j(\mathbf{x})$ are monomials in the space $\mathbf{x}^T = [x, y]$ and $a_j(\mathbf{x})$ are unknown. In the two-dimensional domain, a linear basis could be

$$\mathbf{p}^T(\mathbf{x}) = [1,\ x,\ y]\ , \quad m = 3,$$

while a quadratic basis could be

$$\mathbf{p}^T(\mathbf{x}) = [1,\ x,\ y,\ x^2,\ xy,\ y^2]\ , \quad m = 6$$

The coefficients $\mathbf{a}(x)$ are evaluated by minimizing a quadratic functional J

$$J = \sum_{I}^{n} w(\mathbf{x} - \mathbf{x}_I)[\mathbf{p}^T(\mathbf{x}_I) \cdot \mathbf{a}(\mathbf{x}) - u_I]^2 \tag{2}$$

where $w(\mathbf{x} - \mathbf{x}_I)$ is a weight function and represents the range of influence of node I at the location $\mathbf{x}$.

The minimization of J with respect to $\mathbf{a}(x)$ leads to

$$A(\mathbf{X}) \cdot a(\mathbf{X}) = B(\mathbf{X}) \cdot \boldsymbol{u} \tag{3}$$

$$a(\mathbf{X}) = A^{-1}(\mathbf{X}) \cdot B(\mathbf{X}) \cdot \boldsymbol{u} \tag{4}$$

where

$$A(\mathbf{X}) = \sum_{I}^{n} w_I(\mathbf{X}) \cdot p^T(\mathbf{X}_I) \cdot p(\mathbf{X}_I) \tag{5}$$

$$B(\mathbf{X}) = \left[w_1(\mathbf{X}) \cdot p(\mathbf{X}_1), w_2(\mathbf{X}) \cdot p(\mathbf{X}_2), ..., w_n(\mathbf{X}) \cdot p(\mathbf{X}_n) \right] \tag{6}$$

$$\boldsymbol{u}^T = \left[u_1, u_2, ..., u_n \right] \tag{7}$$

The interpolant $u^h(\mathbf{x})$ can then be represented in terms of shape functions $\phi(x)$:

$$u^h(\mathbf{x}) = \sum_{I}^{n} \sum_{j}^{m} p_j(\mathbf{x}) \cdot \left(A^{-1}(\mathbf{x}) \cdot B(\mathbf{x}) \right)_{I,j} \cdot u_I \equiv \sum_{I}^{n} \phi_I(\mathbf{x}) \cdot u_I \tag{8}$$

The weight function criterion is defined as:

$$w(\boldsymbol{x} - \boldsymbol{x}_I) \equiv w_I(d_I) \tag{9}$$

where

$$d_I = \|\boldsymbol{x} - \boldsymbol{x}_I\| \tag{10}$$

is assumed to be continuous for the first m derivatives with respect to d, specifically stated in the form

$$w_I(\boldsymbol{X}) \equiv w_I(d_i^{2k}) \tag{11}$$

The most frequently used weight functions are:

a) Exponential form function

$$w_I(d_I^{2k}) = \left\{ \frac{e^{-(d_I/c)^{2k}} - e^{-(d_{mI}/c)^{2k}}}{(1 - e^{-(d_{mI}/c)^{2k}})} \right\}, \quad d_I \leq d_{mI} \tag{12}$$

$$w_I(d_I^{2k}) = 0, \quad d_I > d_{mI}$$

b) Conical form function

$$w_I(d_I^{2k}) = 1 - (d_I/d_{mI})^{2k}, \quad d_I \leq d_{mI} \tag{13}$$

$$w_I(d_I^{2k}) = 0, \quad d_I > d_{mI}$$

where c is a constant to control relative weights, and d_{mI} is the size of the support for the weight function $w_I(d)$ - it defines the range of influence of $\mathbf{x}_I$.

Other weight functions frequently mentioned in the literature are the Gaussian and Cubic forms.

The problem formulation features a Galerkin Variational Form with Lagrange Multipliers. For a simple problem for a body with linear elastic behavior, in the domain Ω and boundary Γ, the problem can be stated as

$$\nabla \cdot \boldsymbol{\sigma} + \mathbf{b} = 0 \quad \text{in } \Omega \tag{14}$$

where $\boldsymbol{\sigma}$ is the stress tensor corresponding to the displacement field $\mathbf{u}$, and $\mathbf{b}$ is the force vector acting on the body. The boundary conditions for the problem are given as:

$$\boldsymbol{\sigma} \cdot \mathbf{n} = \bar{t} \quad \text{on } \Gamma_t \tag{15}$$
$$\mathbf{u} = \bar{\mathbf{u}} \quad \text{on } \Gamma_u \tag{16}$$

where $\bar{\mathbf{u}}$ and $\bar{t}$ are the prescribed displacements and tractions on the boundaries Γ_u and Γ_t, respectively; and $\mathbf{n}$ is the unit normal to the domain Ω.

The variational, or weak, form of the equilibrium equation can be satisfied by the trial function $\mathbf{u}(\mathbf{x}) \; \varepsilon \; H^1$ and the Lagrange multiplier $\lambda \; \varepsilon \; H^0$, and the test functions $\delta v \; \varepsilon \; H^1$ and $\delta \lambda \; \varepsilon \; H^0$, ($H^1$ and H^0 refer to Sobolev spaces of degrees 1 and 0):

$$\int_\Omega \delta(\nabla_s \boldsymbol{v}) : \boldsymbol{\sigma} \; d\Omega \; - \int_\Omega \delta v^T \cdot \boldsymbol{b} \; d\Omega \; - \int_{\Gamma_t} \delta v^T \cdot \bar{t} \; d\Gamma \; -$$
$$\int_{\Gamma_u} \delta \boldsymbol{\lambda}^T \cdot (\boldsymbol{u} - \bar{u}) \; d\Gamma \; - \int_{\Gamma_u} \delta v^T \cdot \boldsymbol{\lambda} \; d\Gamma \; = 0 \tag{17}$$

where λ is evaluated to satisfy equation (17). In order to obtain the discrete representation from above, the trial and test functions are structured as in equation (8). The Lagrange multiplier λ is expressed in terms of the arc-length (s) interpolants (N, (s)) along the boundary,

$$\lambda(x) = N_I(s) \; \lambda_I$$

$$\delta \lambda(x) = N_I(s) \; \delta \lambda_I \; , \quad x \in \Gamma_u \tag{18}$$

Substitution of trial and test functions into equation (17) yields the final discrete equation in matrix form:

$$\begin{bmatrix} K & G \\ G^T & 0 \end{bmatrix} \begin{Bmatrix} u \\ \lambda \end{Bmatrix} = \begin{Bmatrix} f \\ q \end{Bmatrix} \tag{19}$$

where

$$K_{IJ} = \int_\Omega B_I^T D B_J \; d\Omega \tag{20}$$

12

$$G_{IK} = -\int_{\Gamma_u} \Phi_I N_K \, d\Gamma \tag{21}$$

$$f_I = \int_{\Gamma_t} \Phi_I \, \bar{t} \, d\Gamma + \int_{\Omega} \Phi_I \, b \, d\Omega \tag{22}$$

$$q_K = -\int_{\Gamma_u} N_K \bar{u} \, d\Gamma \tag{23}$$

and

$$B_I = \begin{bmatrix} \Phi_{I,x} & 0 \\ 0 & \Phi_{I,y} \\ \Phi_{I,y} & \Phi_{I,x} \end{bmatrix} \tag{24}$$

$$N_K = \begin{bmatrix} N_K & 0 \\ 0 & N_K \end{bmatrix} \tag{25}$$

$$D = \frac{E}{1-v^2} \begin{bmatrix} 1 & v & 0 \\ v & 1 & 0 \\ 0 & 0 & \frac{1-v}{2} \end{bmatrix} \quad \text{for plane stress} \tag{26}$$

The Extended Finite Element Method (X-FEM)

X-FEM consists of a standard FEM representation for most of the domain, combined with a set of enriched elements featuring additional degrees of freedom (DOF) in a sub-domain vicinity of a discontinuity, or crack [14-22].

In X-FEM, a discontinuity can be represented independently of the mesh; therefore, re-meshing is not needed during simulation. The discontinuity can be represented by the following enrichment functions:
   a) a Heaviside function (+/-1) defining a jump in displacement across the crack line;
   b) two asymptotic functions near the crack tip field. This field is defined in a local polar coordinate system and is composed of four enrichment functions, with one being discontinuous.

13

X-FEM formulation

The discrete interpolant trial function $u^h(\mathbf{x})$ representation is of the form:

$$u^h(x) = \sum_{i \in I} N_i(x) \cdot u_i + \sum_{j \in J} N_j(x) \cdot H(x) \cdot a_j + \sum_{k \in K} N_k(x) \left(\sum_{l=1}^{4} F_l(x) \cdot b_k^l \right) \tag{27}$$

and the test function is

$$w^h(x) = \sum_{i \in I} N_i(x) \cdot u_i + \sum_{j \in J} N_j(x) \cdot H(x) \cdot c_j + \sum_{k \in K} N_k(x) \left(\sum_{l} F_l(x) \cdot e_k^l \right) \tag{28}$$

where the first term in each equation is the standard FEM interpolation, the second term is for the nodes in elements that are fully cut by the crack, and the third term is for the nodes of the elements containing the crack tip. Additionally:

- $N_j(x)$ are the classical shape functions for the nodes in the domain;
- $H(x)$ is the Heaviside step enrichment function, it is of different sign on opposite sides of the crack; this function models the strong discontinuities;
- $F_j(x)$ are the near-tip enrichment functions which can be defined in local polar coordinates as:

$$\{F_l(r,\theta)\}_{l=1}^{4} = \left\{ \sqrt{r}\cos(\theta/2), \sqrt{r}\sin(\theta/2), \sqrt{r}\sin(\theta/2)\sin(\theta), \sqrt{r}\cos(\theta/2)\sin(\theta) \right\}$$

  r and ϑ are defined by the relative orientation and position of x with respect to the crack. This function models the weak discontinuities.
- a, b, c and e are the generalized coordinates

The local polar coordinates r and ϑ are calculated by the Level Set Method [23] [which tracks the crack propagation. Figure 3 [21] shows the orientation parameters, as defined in the Level Set Method.
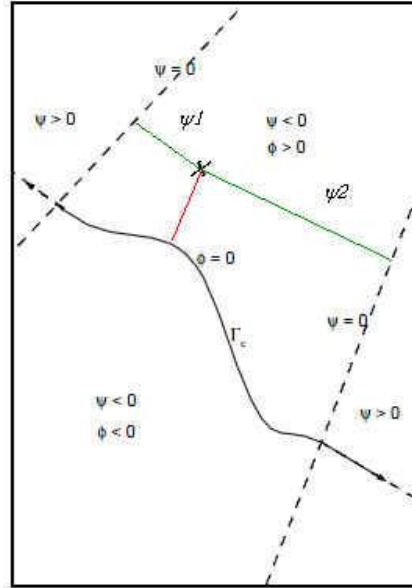
Figure 3 – The Level Set Method

$$\phi = (\boldsymbol{X} - \boldsymbol{X}_\Gamma) \cdot \boldsymbol{n}$$
$$\psi = \boldsymbol{max(\,\psi_1, \psi_2\,)} \tag{29}$$

The Heaviside function is defined as

$$H = sign(\phi) = \begin{Bmatrix} +1 & \phi > 0 \\ -1 & \phi < 0 \end{Bmatrix} \tag{30}$$

And for the near-crack tip alignment

$$r = \sqrt{(\phi^2 + \psi^2)}$$
$$\theta = \tan(\phi/\psi) \tag{31}$$

The components of the weak form discontinuity function (near crack tip) are graphically shown in Figure 4 [21].

(a) $\sqrt{r} \cos\left(\frac{\theta}{2}\right)$ (b) $\sqrt{r} \sin\left(\frac{\theta}{2}\right)$

(c) $\sqrt{r} \sin\left(\frac{\theta}{2}\right) \sin\theta$ (d) $\sqrt{r} \cos\left(\frac{\theta}{2}\right) \sin\theta$
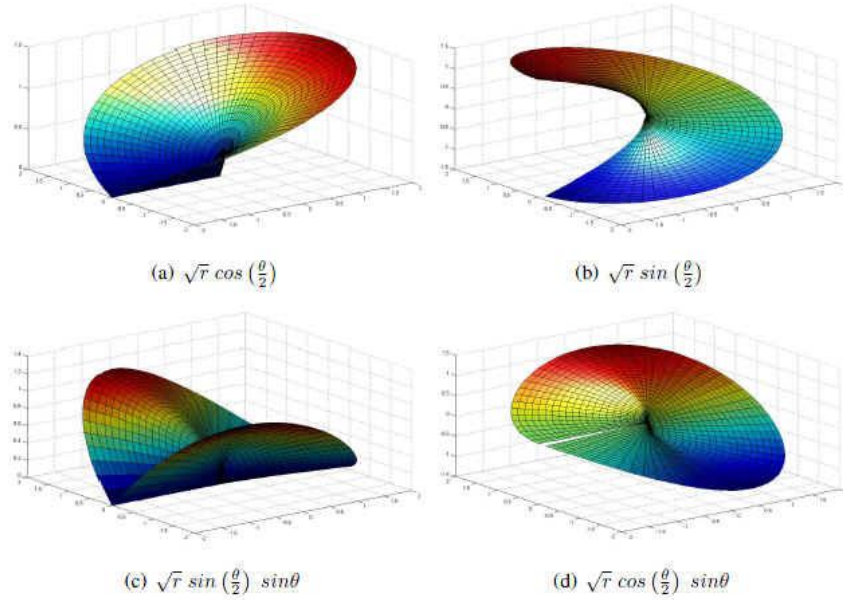
Figure 4 – Weak form discontinuity function

As in the EFGM, the X-FEM formulation for a linear elasto-static model is as follows:

- A body, with domain Ω and outer boundary Γ, is subjected to uniform body/volume forces **b**. Traction forces are applied at boundary Γ_t, and displacement boundary conditions are applied to the boundary surface Γ_u. The body contains a crack surface boundary inside of the domain Ω, Γ_d. The crack tip is treated as traction free at two coincident boundaries Γ_d^+ *and* Γ_d^- .

- The strong form of the equilibrium equation is,

$$\nabla \cdot \sigma + b = 0 \ \ \text{in } \Omega \tag{32}$$

subject to the following boundary conditions

$$\sigma \cdot n = \bar{t} \quad ,on \quad \Gamma_t \tag{33}$$

$$\sigma \cdot n = 0 \quad , \ on \quad \Gamma_d^+ \tag{34}$$

$$\sigma \cdot n = 0 \quad , \ on \quad \Gamma_d^- \tag{35}$$

$$u = \bar{u} \quad , \ on \quad \Gamma_u \tag{36}$$

For small strains and displacements, the linear strain / displacement relationship is expressed as

$$\boldsymbol{\varepsilon} = \nabla_s \boldsymbol{u} \tag{37}$$

Hooke's law for linear elastic materials expresses the stress / strain relationship as

16

$$\boldsymbol{\sigma} = C\,\boldsymbol{\varepsilon}\ ,\quad C \text{ is the elastic stiffness tensor} \tag{38}$$

The weak form of the equilibrium equation is expressed as:

$$\int_{\Omega}\left[\nabla w : \sigma(u)\right] d\Omega - \int_{\Gamma_t} w\cdot \bar{t}\ d\Gamma - \int_{\Omega} w\cdot b\ d\Omega = 0 \tag{39}$$

Expanding Equation (39) with the test function (Equation (28)) and trial function (Equation (27)) and reducing ultimately leads to the discrete form

$$-\int_{\Omega}(B^u_{std_i})^T \sigma\ d\Omega + \int_{\Gamma_t}(N^u_{std_i})^T\ \bar{t}\ d\Gamma + \int_{\Omega}(N^u_{std_i})^T\ b\ d\Omega = 0$$

$$-\int_{\Omega}(B^a_{enr_i})^T \sigma\ d\Omega + \int_{\Gamma_t}(N^a_{enr_i})^T\ \bar{t}\ d\Gamma + \int_{\Omega}(N^a_{enr_i})^T\ b\ d\Omega = 0 \tag{40}$$

$$-\int_{\Omega}(B^b_{enr_i})^T \sigma\ d\Omega + \int_{\Gamma_t}(N^b_{enr_i})^T\ \bar{t}\ d\Gamma + \int_{\Omega}(N^b_{enr_i})^T\ b\ d\Omega = 0$$

For our linear elastic material, we use Hooke's stress/strain relation in equation (38) and the small strain/displacement relation in equation (37). The discrete form of the static equilibrium equation reduces to:

$$K_{ij}\ d_j = f_i \tag{41}$$

where d_j is the displacement vector. The stiffness matrix elements are:

$$K^{\alpha\beta}_{ij} = \int_{\Omega}(B^{\alpha}_i)^T C(B^{\beta}_j) d\Omega,\quad (\alpha,\beta = u,a,b) \tag{42}$$

where B is the gradient operator given as:

$$B^u_i = B^u_{std_i} = \begin{bmatrix} (N_{std_i})_{,x} & 0 \\[2mm] 0 & (N_{std_i})_{,y} \\[2mm] (N_{std_i})_{,y} & (N_{std_i})_{,x} \end{bmatrix} \tag{43a}$$

$$B^a_i = B^a_{enr_i} = \begin{bmatrix} (HN_{std_i})_{,x} & 0 \\[2mm] 0 & (HN_{std_i})_{,y} \\[2mm] (HN_{std_i})_{,y} & (HN_{std_i})_{,x} \end{bmatrix}$$

$$B_i^{bl} = B_{enr_i}^{bl} = \begin{bmatrix} (F_l N_{std_i}),_x & 0 \\ 0 & (F_l N_{std_i}),_y \\ (F_l N_{std_i}),_y & (F_l N_{std_i}),_x \end{bmatrix}, \quad (l = 1, 4) \tag{43b}$$

The complete external force vector f_I is defined by:

$$f_i = \left\{ f_i^u, f_i^a, f_i^{b1}, f_i^{b2}, f_i^{b3}, f_i^{b4} \right\} \tag{44}$$

where

$$f_i^u = \int_{\Gamma_i} (N_{std_i})^T \ \bar{t} \ d\Gamma + \int_\Omega (N_{std_i})^T \ b \ d\Omega$$

$$f_i^a = \int_{\Gamma_i} (N_{enr_i}^a)^T \ \bar{t} \ d\Gamma + \int_\Omega (N_{enr_i}^a)^T \ b \ d\Omega \quad , (l = 1, 4)$$

$$f_i^{bl} = \int_{\Gamma_i} (N_{enr_i}^{bl})^T \ \bar{t} \ d\Gamma + \int_\Omega (N_{enr_i}^{bl})^T \ b \ d\Omega$$

Evaluation Methodology

The selected software for this study is LS-DYNA, marketed by Livermore Software Technology Corp. (LSTC). This software is commercially available and is built around the DYNA3D and NIKE3D Finite Element codes developed at the Lawrence Livermore National Laboratories. LS-DYNA features both the EFGM and the X-FEM for simulating the initiation and propagation of cracks in Elasto-plastic materials. A total of four licenses were purchased in order to execute parallel runs on up to four CPUs.

The two methodologies require unique geometric representation of the chosen ship model: The X-FEM requires a fine mesh definition around the expected area of collision. Shell type elements are used which require a material-cohesive-formulation that describes a trilinear traction-separation law, where the traction components drop to zero when separation reaches a specified limit. Special nodal constraints along the boundary between the X-FEM elements and the conventional shell elements are used to preserve continuity.

The EFGM, as currently implemented in LS-DYNA, does not use shell elements. This requires mesh definition in the form of tetrahedral elements and a minimum of three elements through the plate thickness; additionally, the minimum required aspect ratio of the elements must be preserved in order to prevent an excessively stiff response. The EFGM also requires the use of a material-

18

cohesive formulation as described previously. This mesh sub-division significantly increases the number of degrees of freedom and, consequently, the size of the problem and computation time.

A pre-processor was developed to specify the geometric definition around the location of ice impact and its corresponding load history. This pre-processor needs as input only the hull surface definition, the location and conditions of the ice load and the method (Baseline FEM, EFGM or X-FEM) being used. A flow diagram of the algorithm and its source code are included in Appendix B.

A Test Matrix was designed for the evaluation of robustness of these methods and their applicability to modeling the fracture mechanics on the plating of ship hulls subjected to various levels of collision impact by sea ice; these were selected based on Polar Class (PC) descriptions, as defined by the International Association of Classification Societies (IACS). The Glancing Impact Load characteristics for these PCs are derived from parameters defined as the Class Factors [26].

Table 1 – Polar Class Description

Polar Class	Ice Description
PC 1	Year-round operation in all Polar Waters
PC 2	Year-round operation in moderate multi-year ice conditions
PC 3	Year-round operation in second-year ice which may include multi-year inclusions
PC 4	Year-round operation in thick first-year ice which may include old ice inclusions
PC 5	Year-round operation in medium first-year ice which may include old ice inclusions

As a baseline for comparison, the tests included cases run with the standard Finite Element Method.

In order to meet the requirements described in the Statement of Work, the Test matrix includes locations of impact in the area of the hull near the bow and around the shoulder area. At each of these longitudinal locations, the tests further included: an elevation coincident with the waterline, which includes a deck; and an elevation below the waterline that is approximately midway between decks.

The Test Matrix is shown in Table 2.

Table 2 – Test Matrix

Location of Simulated Collision on the Hull (From Forward Perpendicular)		IACS Polar Class				
	(x / Length) : (-z / Draft)	PC1	PC2	PC3	PC4	PC5
Loc 1	0.10 : 0.0	X	X	X	X	X
Loc 2	0.10 : - 0.1	X	X	X	X	X
Loc 3	0.20 : 0.0	X	X	X	X	X
Loc 4	0.20 : - 0.1	X	X	X	X	X
Loc 5	0.4 : 0.0	X	X	X	X	X

A Watson-class Large Medium Speed Roll-On Roll-Off (LMSR) cargo ship hull was selected for testing. Although LMSR type ships do not frequent polar waters and their hulls are not designed or optimized for these environments, their hull definitions are freely available in the public domain with no export control restrictions. For this reason, their selection was recommended for this project since it does not detract from the primary objective of evaluation of advanced methods in fracture mechanics for applicability in hull structures In order to keep the size of the computational models within a workable frame, several simplifications were made:
   a) The section of the hull modeled is below the 3.0 meter above the waterline elevation.
   b) Only the Port side of the hull is modeled.
   c) Only three decks are modeled: at 2.0 meters above the waterline, at the waterline and at -2.0 meters below the waterline.
   d) Ten transverse bulkheads are modeled.
   e) Vertical Stanchions are placed along the symmetry plane in order to account for the structural strength of the starboard side of the ship, which is not modeled.
   f) The structural model is unconstrained in all six degrees of freedom in order to provide for inertial (i.e. rigid body) response to the collision forces. The rigid body response is the zero frequency secular response of the structure to external loading. It is inertially coupled to the structural response. The rigid body mass and moment of inertia are the total mass and moment of inertia of the free-free structure modeled.
   g) The hull, decks and bulkheads are modeled to have a uniform "smeared thickness" to be equivalent in strength to that added by scantling, frames, beams and girders.
   h) No hydrodynamic added mass effects or fluid interaction effects are modeled.

The Ice Loads are modeled using the algorithm Direct Design for Polar Ships (DDPS) developed from the International Association of Classification Societies IACS UR for Polar Ships, by Claude Daley [24, 25, 27]. The defining parameters for each of the PC Classes are shown in Table 3.

Table3 – PC Parameters

PC Class Parameters			
	Vs (m/s)	Po (Mpa)	h_ice (m)	sig_f (Mpa)
PC1	5.70	6.00	7.00	1.40
PC2	4.00	4.20	6.00	1.30
PC3	3.00	3.00	4.25	1.20
PC4	2.50	2.45	3.50	1.10
PC5	2.00	2.00	3.00	1.00

A preprocessor was developed and implemented for the generation of the input data for each run (Appendix B). It uses as input the surface definition of the hull, the longitudinal and elevation coordinates of the impact location, and intensity level of collision (graded by IACS rules as PC1 Class through PC5 Class). As output, the preprocessor generates the mesh for the hull and the rest of the structure, such as the decks, bulkheads and stanchions. It also generates the load from the collision of hull and sea ice; this load is defined for an area of the hull which is dependent on the position and intensity of impact, and is time and orientation dependent. The duration of the simulation is also calculated; it depends on the relative location of impact and the initial relative

20

velocity of the ship; when the relative velocity between ship and sea ice reaches zero, the load is considered to have dissipated and the simulation ends.

The material properties definition for the hull, decks and bulkhead are those of Grade A shipbuilding steel. An elasto-plastic kinematic model is used for modeling the structural behavior of steel. These material properties are shown in Table 4.

Table 4 – Material properties for hull plating

Density (kg/mm^3)	7.83E-06
Young's Modulus (kN/mm^2)	210.
Poisson Ratio	0.3
Yield Strength (kN/mm^2)	0.25
Tangent Modulus	0.01
Hardening parameter	1.0
Maximum tensile strength (kN/mm^2)	0.40
Critical crack opening displacement (dimensionless)	0.50

Results

The calculated ice load history distributions for each of the locations and PC classes are shown in Appendix A, Figures A1 through A20. These load history distributions are determined using the DDPS algorithm; they are applied in the normal orientation to the hull plating. The ice loads are applied as pressure distributed over a nominal contact area; this area is a function of the normal ice indentation and the contact geometry.

The Baseline FEM and the X-FEM methods were run successfully and the results are compared in this section.

The runs using the EFGM were not successful; these require significantly more computational resources than what is available. The extra-fine nodal definition that is required for describing the hull structure geometry in the vicinity of the expected area of collision limits the size of the maximum time step for obtaining the solution. This limitation, plus the very large number of degrees of freedom, made the testing non-feasible for parallel processing in four CPUs. The estimated computation time for the solver to execute one test case is greater than 58,000 minutes (> 40 days).

The maximum nodal displacements and maximum plastic strains are used as metrics for comparison of the Baseline FEM and the X-FEM results for each of the cases described in the Test Matrix. The results of the maximum nodal displacements and maximum plastic strain for the Baseline FEM runs are shown in Table 5; the results for the X-FEM runs are shown in Table 6. The nodal displacements include, in addition to the deformation displacements, inertial responses of translational and rotational motions of the center of mass of the ship hull structure due to the impact loads.

For simplicity of reference, the run labels are constructed as "PC(Class)_(location)_(method). For example: a run simulating a collision class level 3, at location 2, using the X-FEM method is referenced as "PC3_2_XFEM". This nomenclature will be used through the rest of this report.

The generated mesh of the structure of the model, for the Baseline FEM and X-FEM runs, is shown in isometric views from the starboard side in Figures 5 and 6, it shows the decks, bulkheads and stanchions; the port side, in close up, of the hull is shown in Figure 7, the red color area shows the finer mesh definition around the collision region. The selected region of collision has a 4 to 1 ratio of element density (relative to the coarser hull meshing elsewhere, shown in color blue).

The generated mesh of the structure for the EFGM runs is shown close-up in Figures 8 and 9; it shows the extreme mesh refinement, with a ratio of element density of 48 to 1. The limitation of tetrahedral element definition for this method requires a minimum of three elements through the plate thickness. Additionally, a minimum aspect ratio must be maintained in order to prevent an excessive stiff response; this subdivision increases significantly the total number of degrees of freedom for the problem. This mesh refinement was based on recommendations by the vendor's support engineering team.

Several time steps of the transient total nodal displacements of the simulation for the run PC2_2_XFEM are shown in Figures 10 through 17. A crack occurs in this run near the area where a transverse bulkhead is positioned; this can be seen in close-up Figures 18 -19. Figures 20 and 21 show the total displacement results for the run PC1-2_FEM; the resulting crack propagation occurs along element boundaries. Plastic strain results are compared for two runs with same conditions but different methods, PC1-2_FEM and PC1-2_XFEM, in Figures 22 and 23, respectively. Finally, Figures 24 through 27 compare the two methods for a condition where the impact area is in the shoulder region of the hull.

Discussion of Results

Comparison of maximum displacement between the Baseline FEM and X-FEM, shown in Tables 5 and 6, indicate that both methods predict comparable values for the same test conditions (PC class and impact location). As indicated earlier, the total calculated displacements represent combined nodal translation of the ship's center of mass (COM) and those relative to the COM. The transient total displacements for the run PC2_2_XFEM are illustrated in Figures 10 through 17; these show the combined rigid-body response of the ship structure and the relative local deformations.

Similarly, the resulting maximum plastic strain levels, in Tables 5 and 6, for any particular test condition are comparable between the two methods. These plastic strain deformations are relative to the initial stress-free local geometry of the elements. Crack initiation and propagation occurs only in those tests with impact levels of PC class 1 and 2; while for test with lesser impact, PC class $3-5$, only structural deformation occurs. In the Baseline FEM, the crack propagation can only occur along element boundaries, while in the X-FEM crack propagation does occur through the enriched X-FEM elements. This difference can be observed in the comparison between Figures 18 and 21.

Evaluation of the EFGM requires more hardware resources than those available for the execution of the present task. The current EFGM implementation in LS-DYNA for only tetrahedral elements is not a practical choice, as described in the Results section. Future plans for implementation of the EFGM with thick shell elements were mentioned by the LS-DYNA support team.

The results from this study show fairly good comparability between the two methods; the plastic strain and total displacement results are generally of the same order of magnitude. The computational time for both methods was also similar, typically between 90 and 120 minutes per run. The capability of X-FEM for better resolution of crack propagation makes it a preferred choice. However, the limited implementation of this method in most commercial structural analysis codes is a factor for consideration in selecting the proper code for the needed application. For applications that require a high level of resolution for modeling crack propagation, the X-FEM is the better method.

Future evaluation of the accuracy of these methods requires comparison against reliable validation data.

Conclusions

This work presents the basis of a modeling framework for future studies of fracture mechanics on ship hulls subjected to impact with large masses of sea ice. The ship hull structural responses, between the Baseline FEM and the X-FEM, to ice loads are reasonably comparable. Computational times between the two methods are also comparable. For studies and analyses that require high degree of predictive modeling of the path of crack propagation, the X-FEM is the recommended method; its capability to model crack propagation through an enriched element offers better resolution than the classical FEM without the need for extreme element sub-division.

The limited implementation of X-FEM in most commercial codes must be a consideration in the selection and acquisition of the proper software package. For studies that do not require a high degree of predictive modeling of crack propagation, the Baseline FEM can provide adequate results.

The proposed next step for this project is the validation and fine tuning of the modeling framework against experimental data.

This page intentionally left blank

Table 5 – Nodal Displacements and Plastic Strains Obtained with the Baseline FEM

Baseline Standard Finite Element Method										
Location of Collision	PC1		PC2		PC3		PC4		PC5	
	max	min	max	min	max	min	max	min	max	min
Displacement (mm)										
Location 1	6424*	6	1498*	11	1381	18	1171	17	1136	20
Location 2	3578*	5	1351*	9	1095	15	1032	15	891	13
Location 3	5773	10	1944	18	997	25	981	26	858	24
Location 4	4855	14	1820	14	1044	23	933	24	902	25
Location 5	73	0	53	1	45	1	41	1	37	1
Plastic Strain										
Location 1	0.800*	0	0.253*	0	0.017	0	0.0108	0	0.009	0
Location 2	0.805*	0	0.253*	0	0.073	0	0.0558	0	0.042	0
Location 3	0.370	0	0.100	0	0.019	0	0.0114	0	0.000	0
Location 4	0.242	0	0.066	0	0.039	0	0.0308	0	0.024	0
Location 5	0.0	0.0	0.0	0.0	0.0	0.0	0.0	0.0	0.0	0.0

* Crack initiation and propagation occurs

Table 6 – Nodal Displacements and Plastic Strains Obtained with the X-FEM

Extended Finite Element Method (X-FEM)										
Location of Collision	PC1		PC2		PC3		PC4		PC5	
	max	min	max	min	max	min	max	min	max	min
Displacement (mm)										
Location 1	6691*	6	1688*	9	1359	13	1143	14	1101	16
Location 2	4001*	3	1729*	9	1124	16	1006	14	862	11
Location 3	7797*	7	2385	17	954	23	942	24	825	22
Location 4	5306	5	2279	9	1439	18	1090	21	960	22
Location 5	74	0	52	1	44	1	41	1	37	1
Plastic Strain										
Location 1	1.13*	0	0.297*	0	0.038	0	0.0186	0	0.0147	0
Location 2	0.81*	0	0.504*	0	0.207	0	0.1394	0	0.0849	0
Location 3	0.78*	0	0.272	0	0.025	0	0.1165	0	0.0054	0
Location 4	0.476	0	0.256	0	0.147	0	0.1007	0	0.0683	0
Location 5	0.023	0	0.004	0	0.014	0	0.010	0	0.002	0

* Crack initiation and propagation occurs

For simplicity of reference, the run labels are constructed as "PC(Class)_(location)_(method). For example: a run simulating a collision class level 3, at location 2, using the X-FEM method is referenced as "PC3_2_XFEM". This nomenclature will be used through the rest of this report.
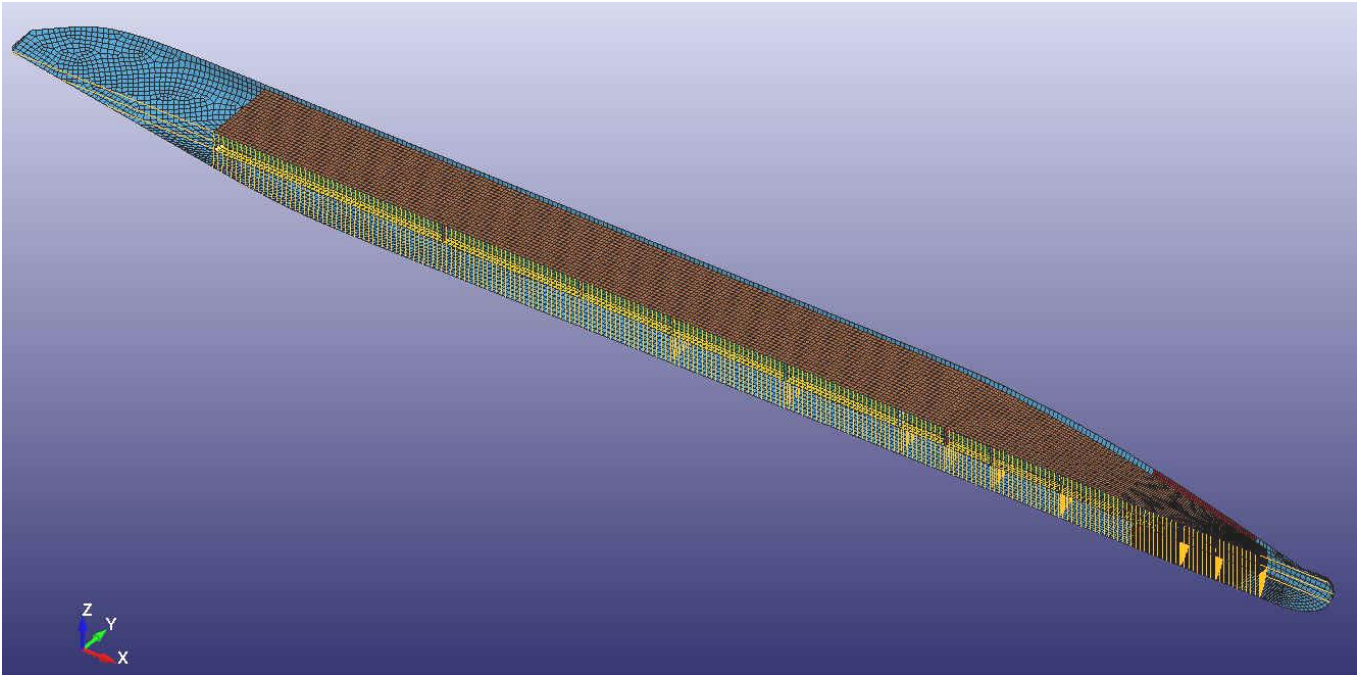
Figure 5 – Isometric view of the model
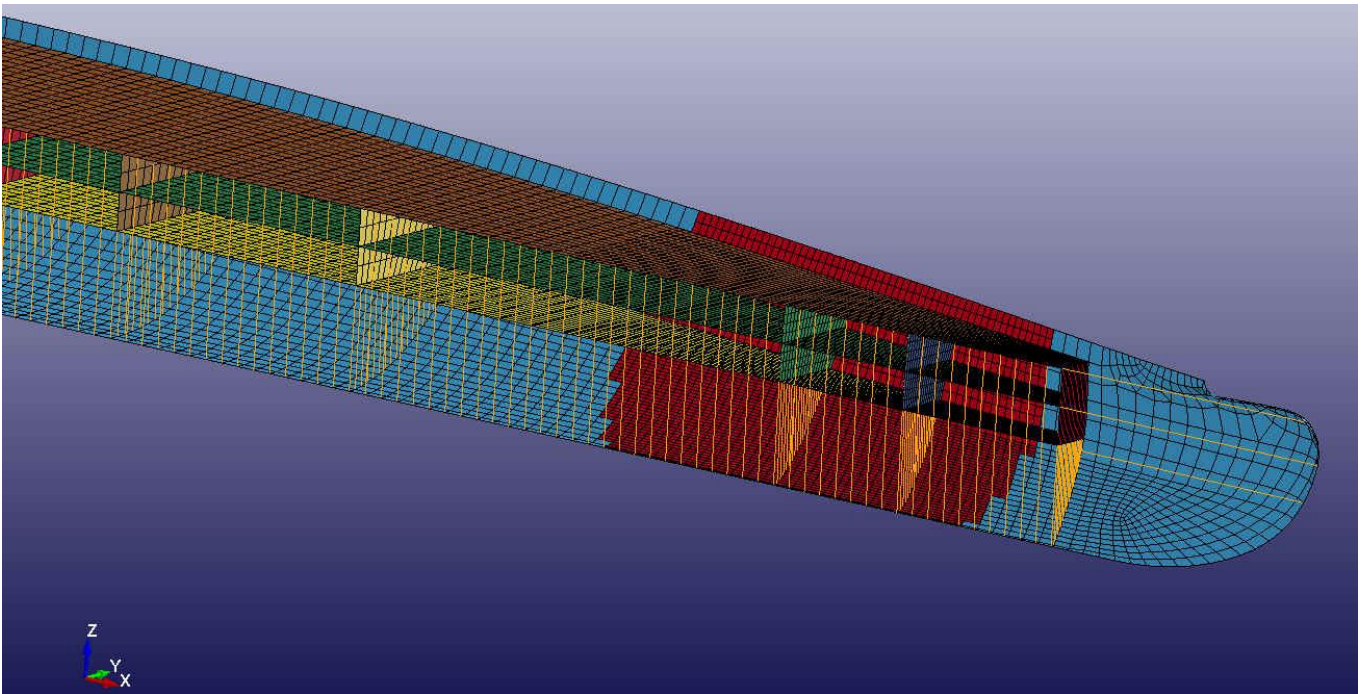
Figure 6 – Isometric Close-up View of the model around expected location of collision
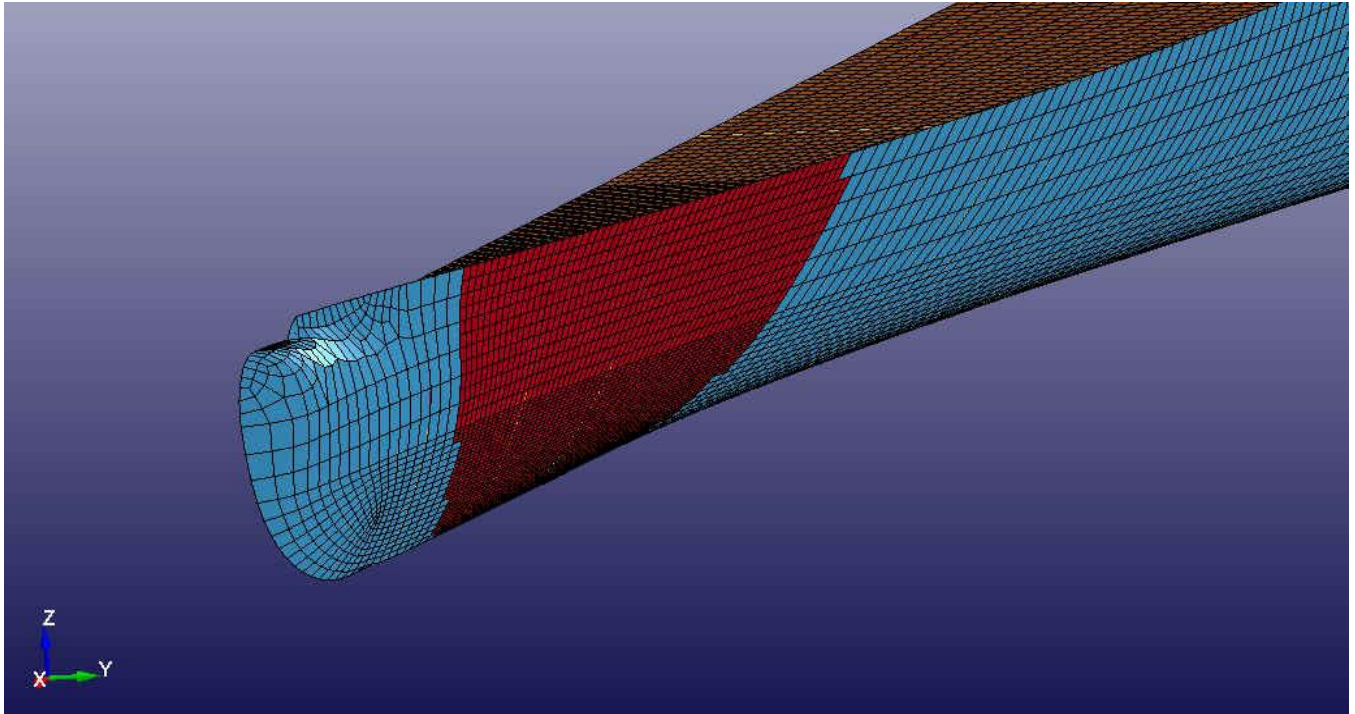
Figure 7 – Isometric Close-up view of port side of the hull
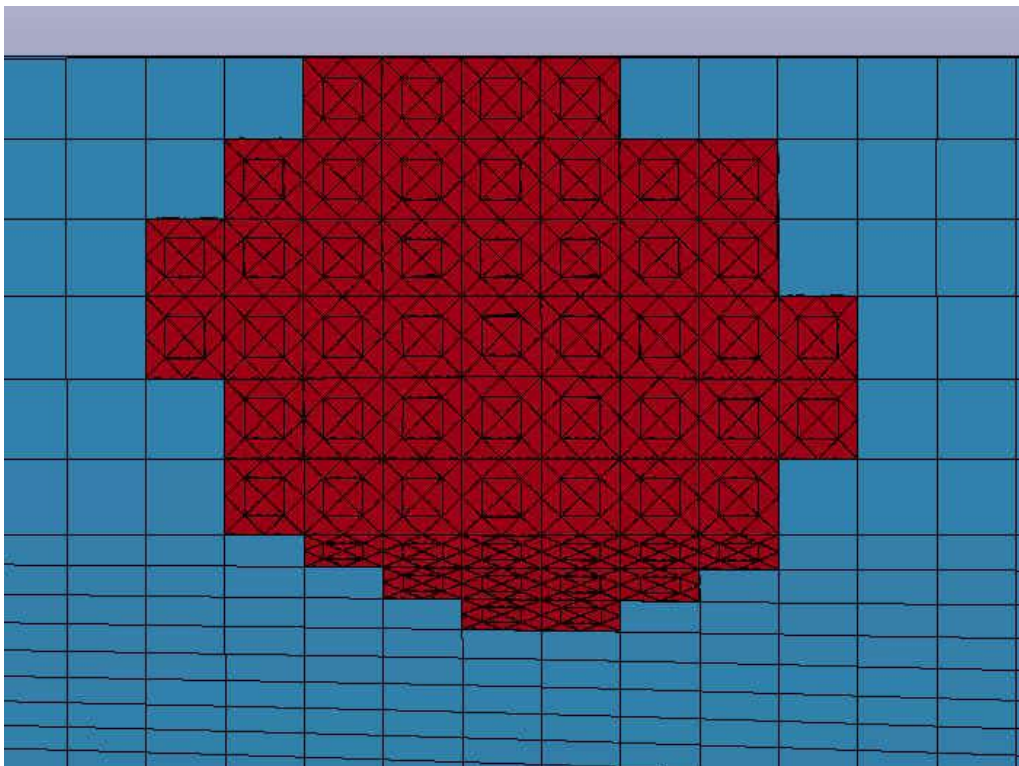
Figure 8 – EFGM: Close-up view of tetrahedral elements around area of collision
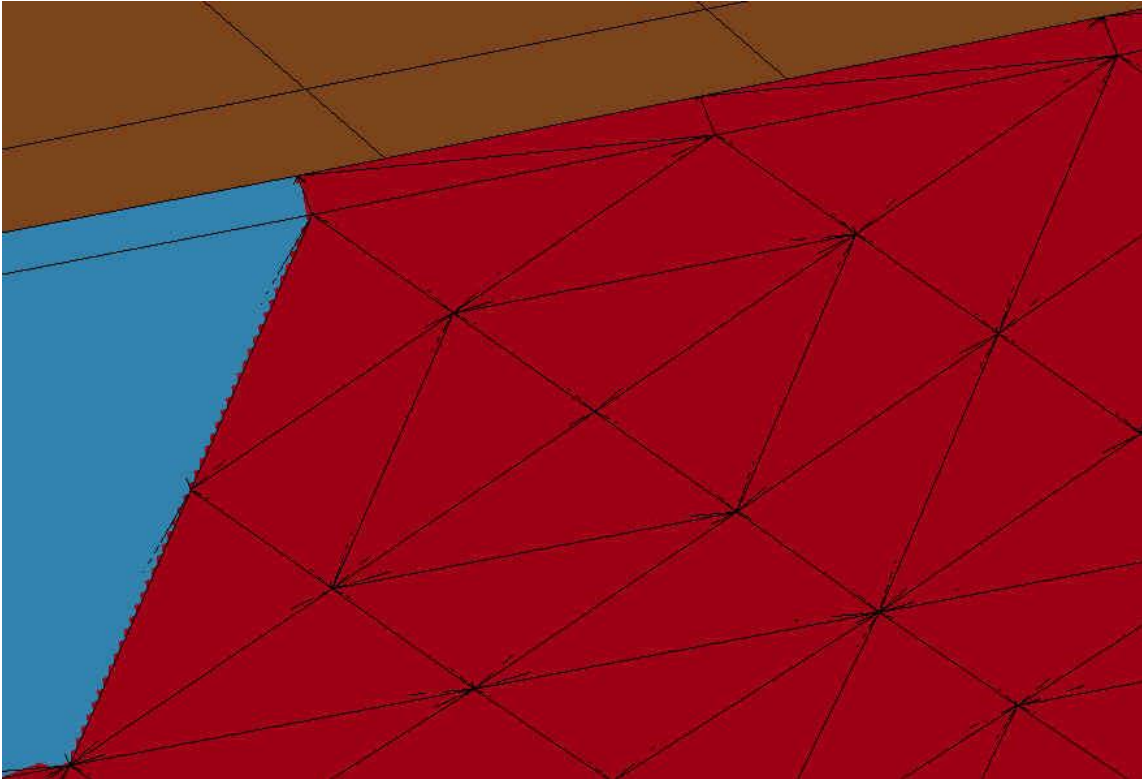
Figure 9 – EFGM: extreme close-up of tetrahedral elements
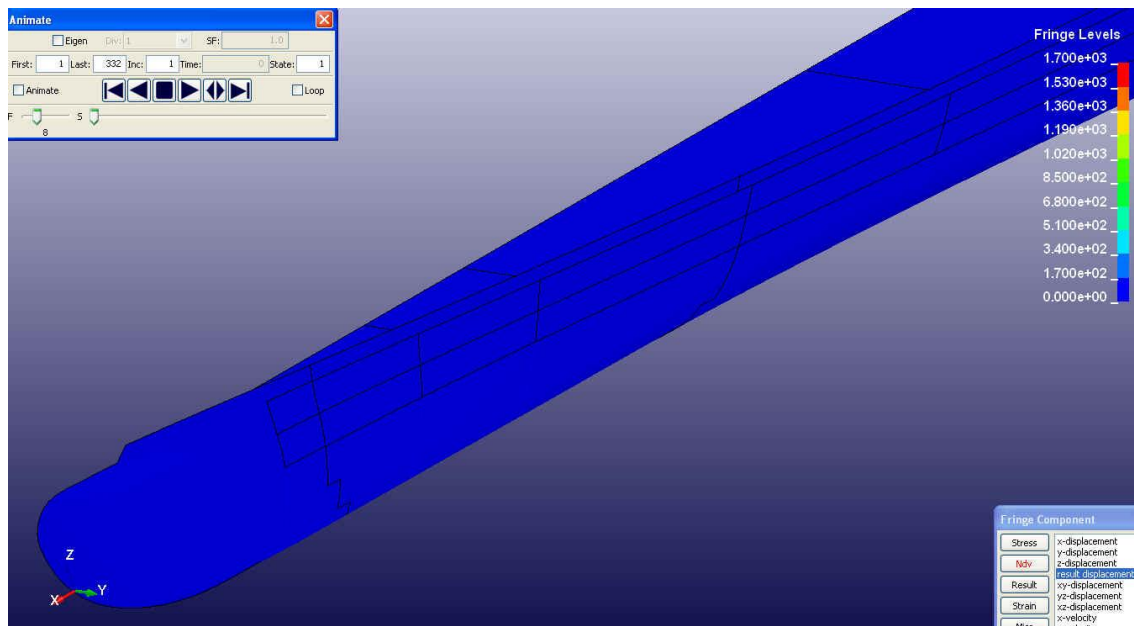
Figure 10 – PC2_2_XFEM Total Displacement (t = 0 millisec.)
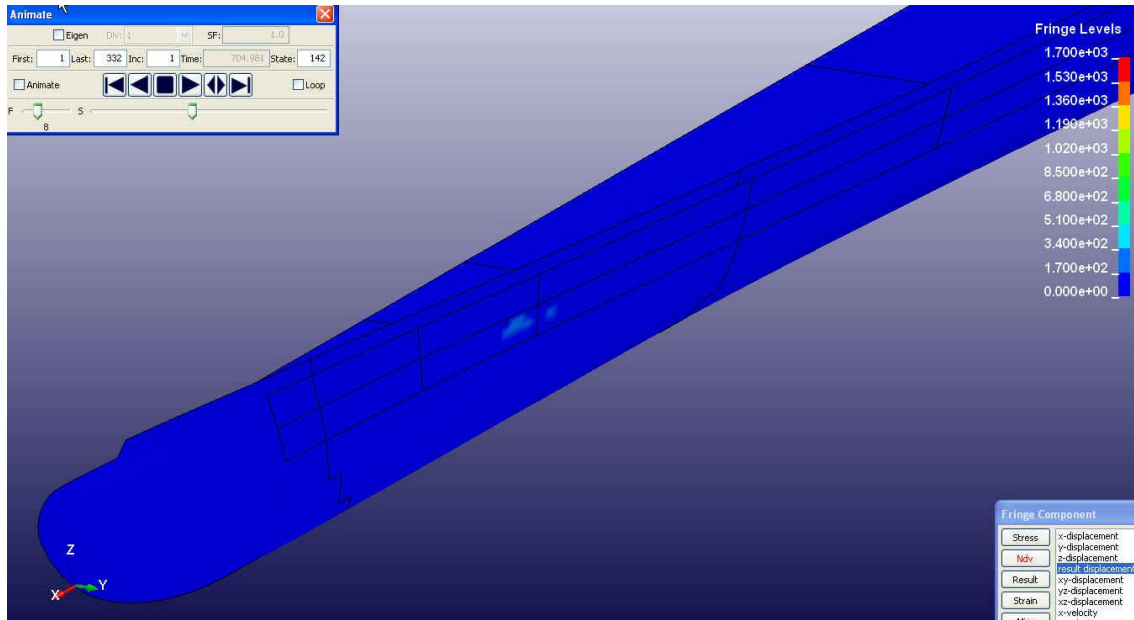
Figure 11 – PC2_2_XFEM Total Displacement (t = 705 millisec)
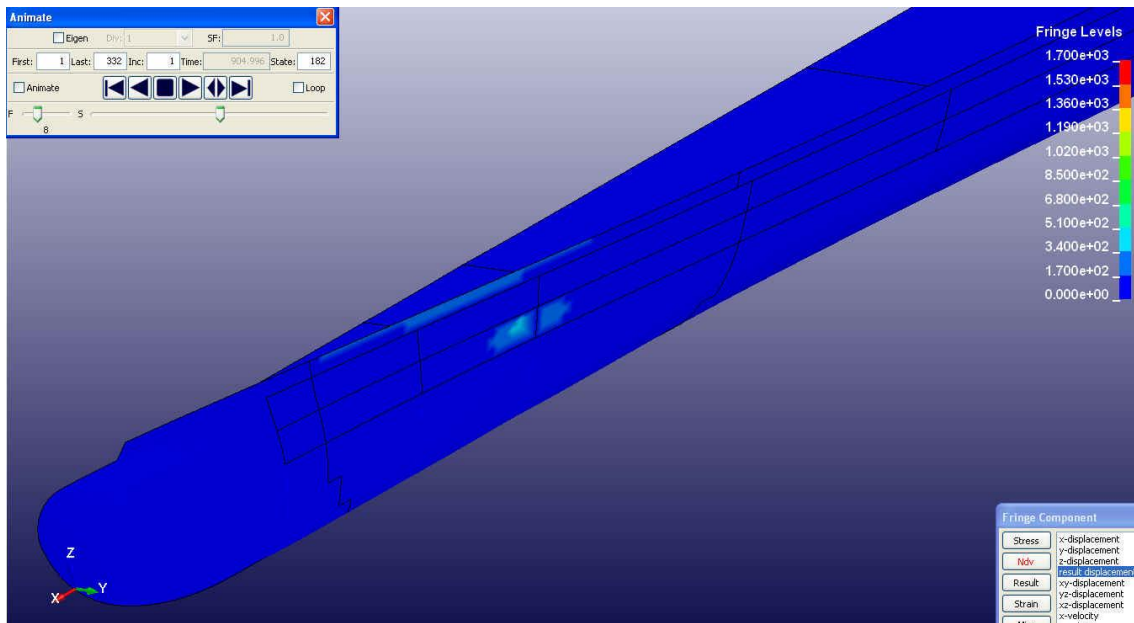
Figure 12 – PC2_2_XFEM Total Displacement (t = 905 millisec)
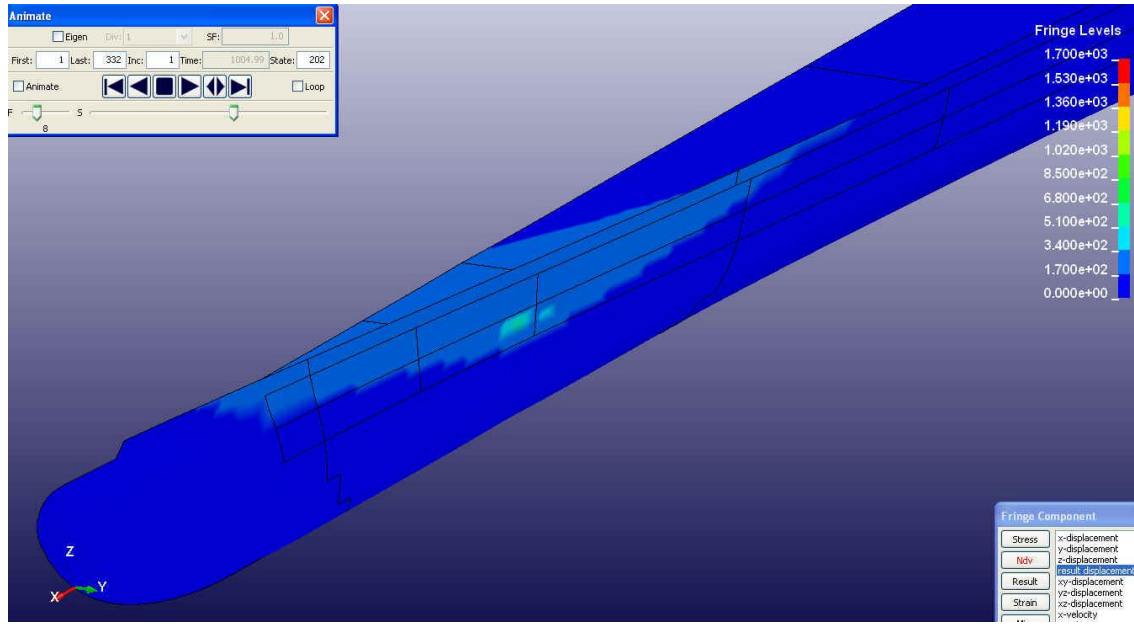
Figure 13 – PC2_2_XFEM Total Displacement (t = 1005 millisec)
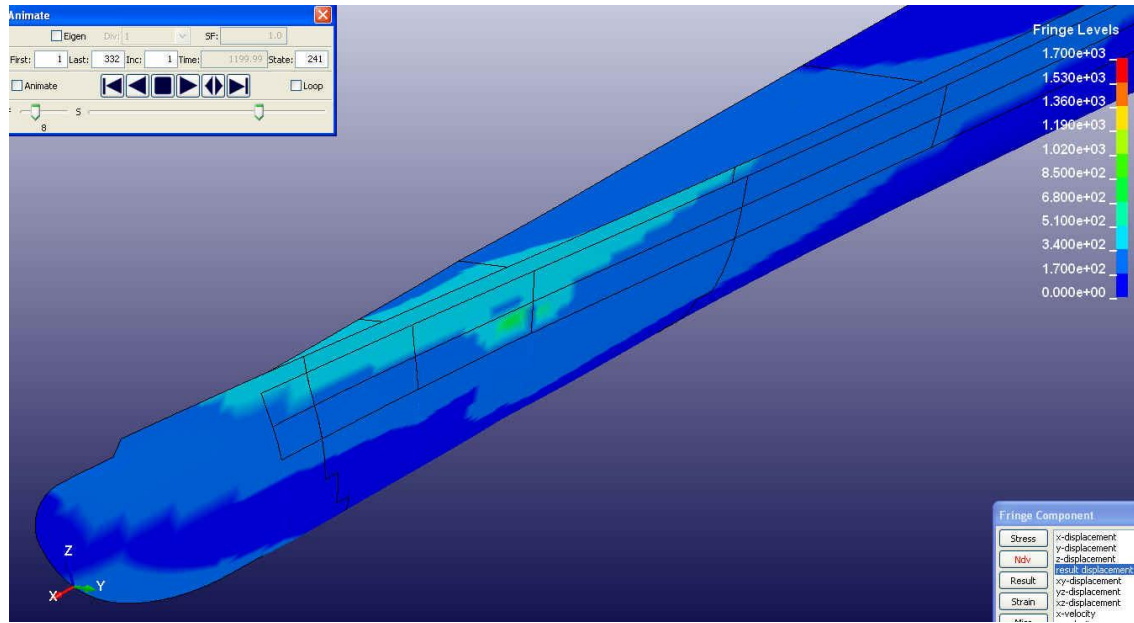
Figure 14 – PC2_2_XFEM Total Displacement (t = 1200 millisec)
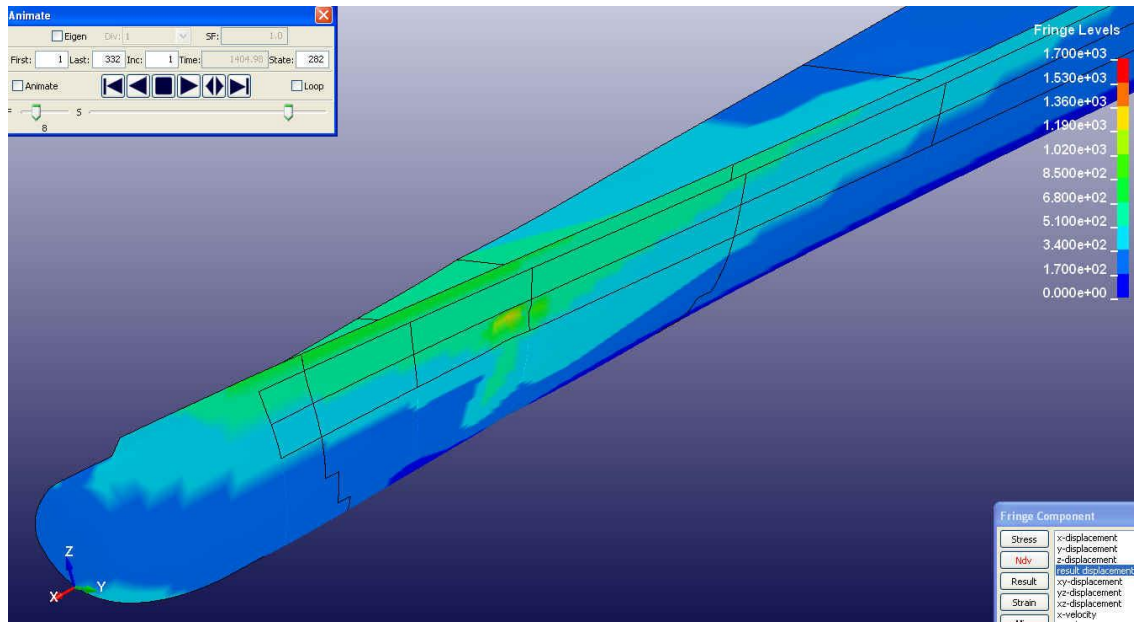
Figure 15 – PC2_2_XFEM Total Displacement (t = 1405 millisec)
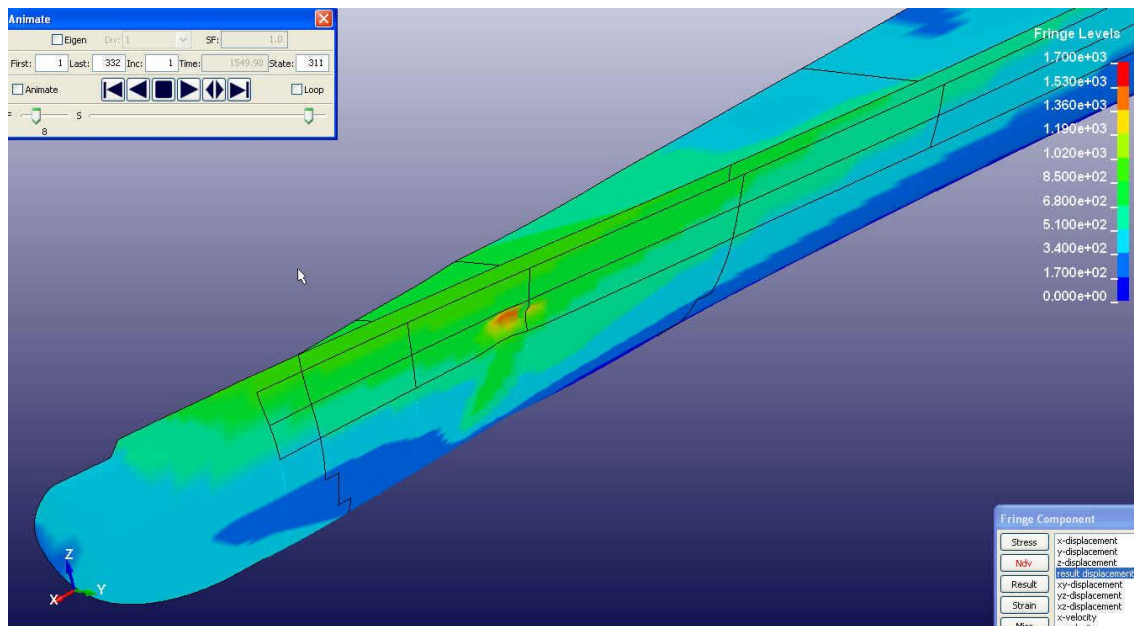
Figure 16 – PC2_2_XFEM Total Displacement (t = 1550 msec)

Figure 17 – PC2_2_XFEM Total Displacement (t = 1650 msec)
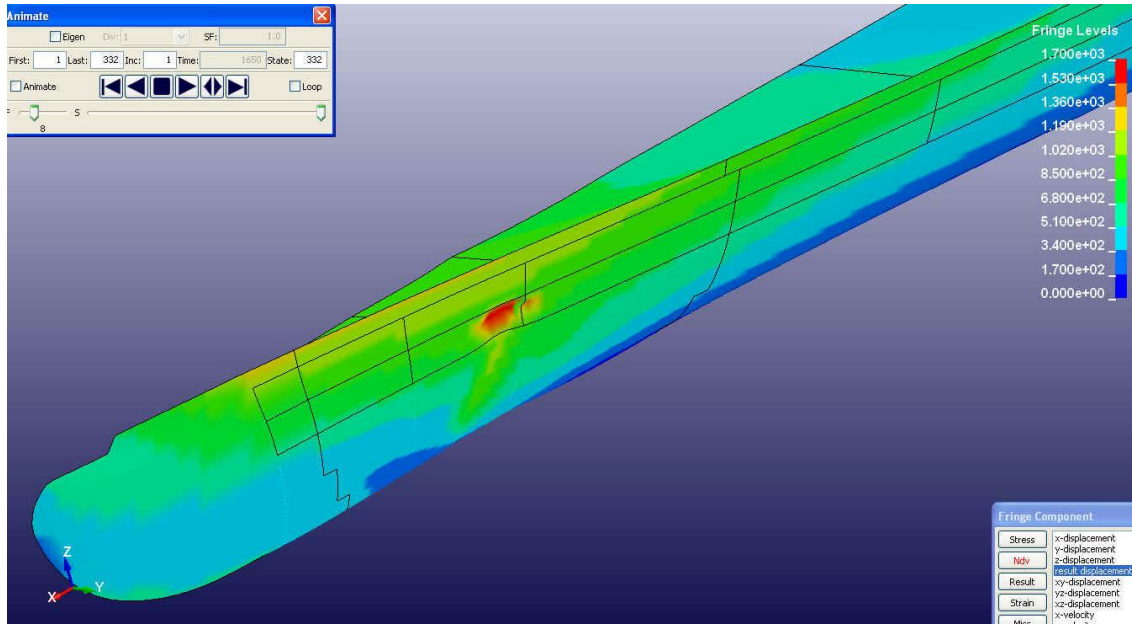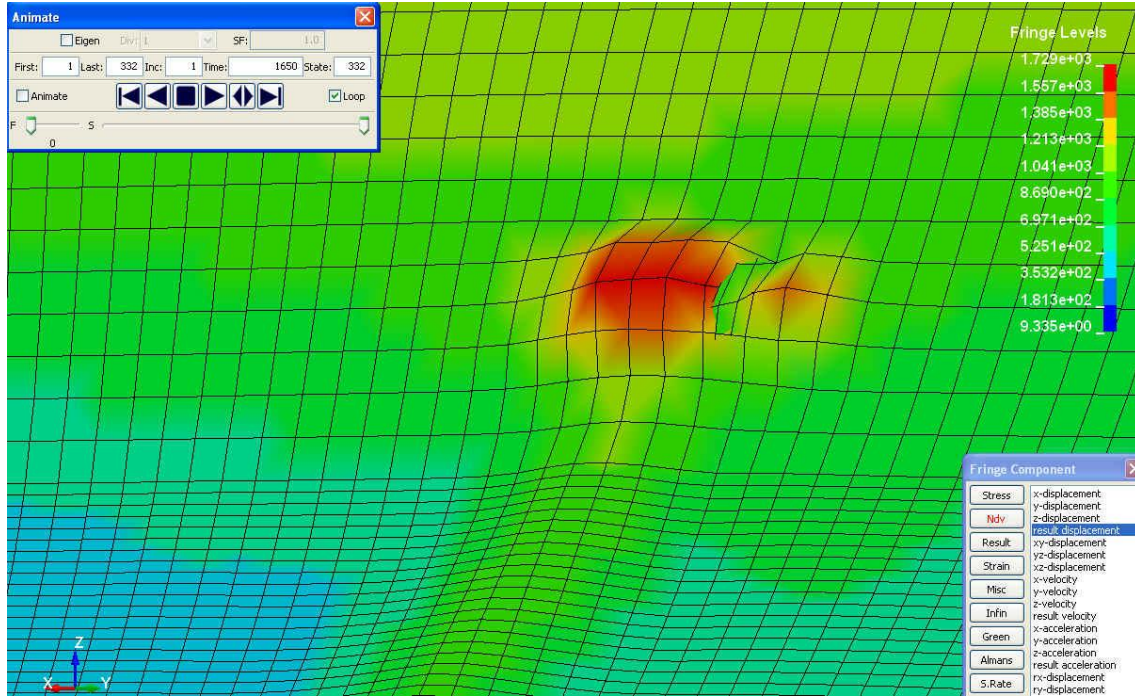
Figure 18 – PC2_2_XFEM Total Displacement – Close-up of crack propagation
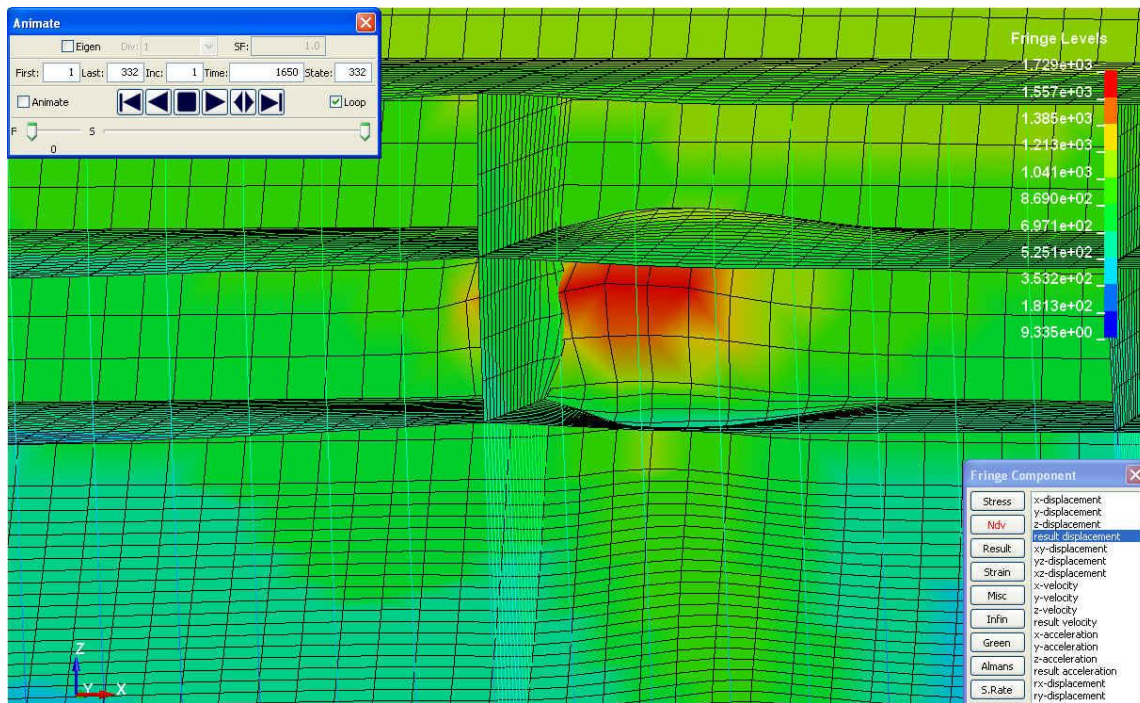
Figure 19 – PC2_2_XFEM Total Displacement – Close-up inside the hull
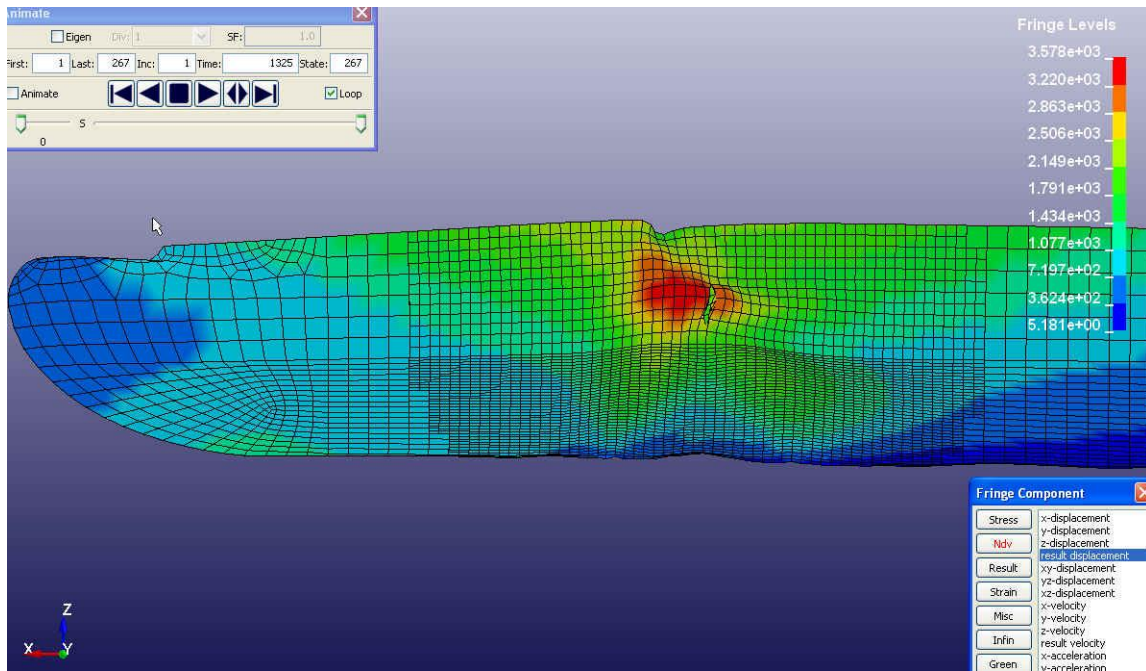
Figure 20 – PC1-2 FEM Total Displacement (crack on element boundary)
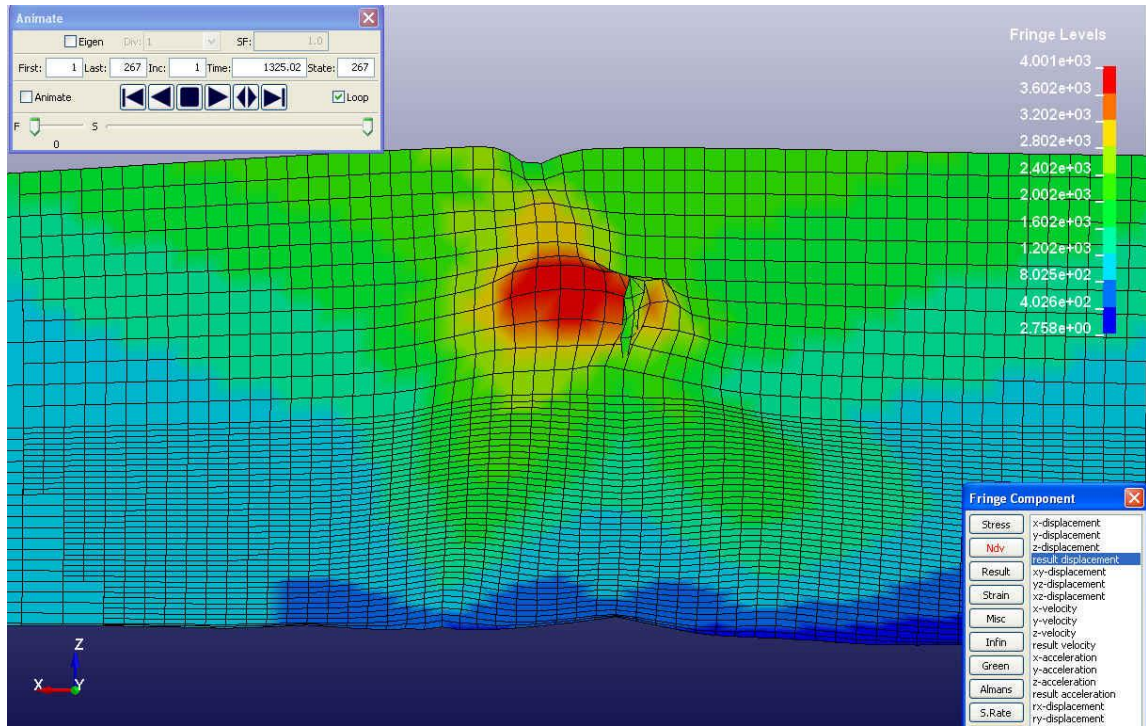
Figure 21 – PC1-2 FEM Total Displacement (close-up)
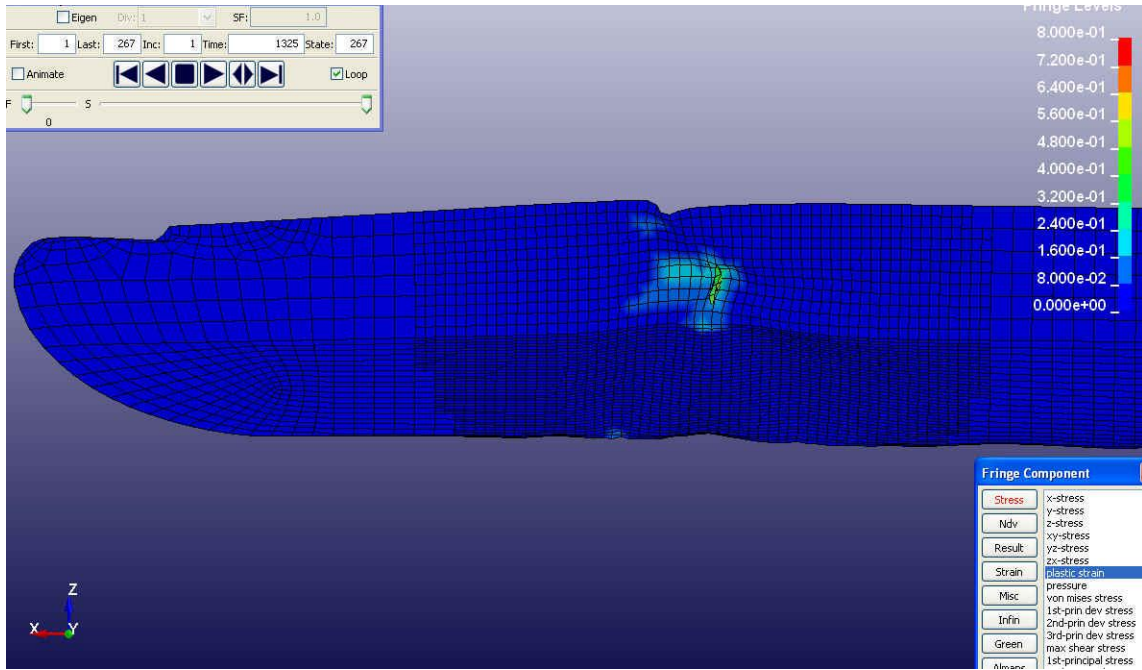
Figure 22 – PC1-2 FEM – Plastic Strain
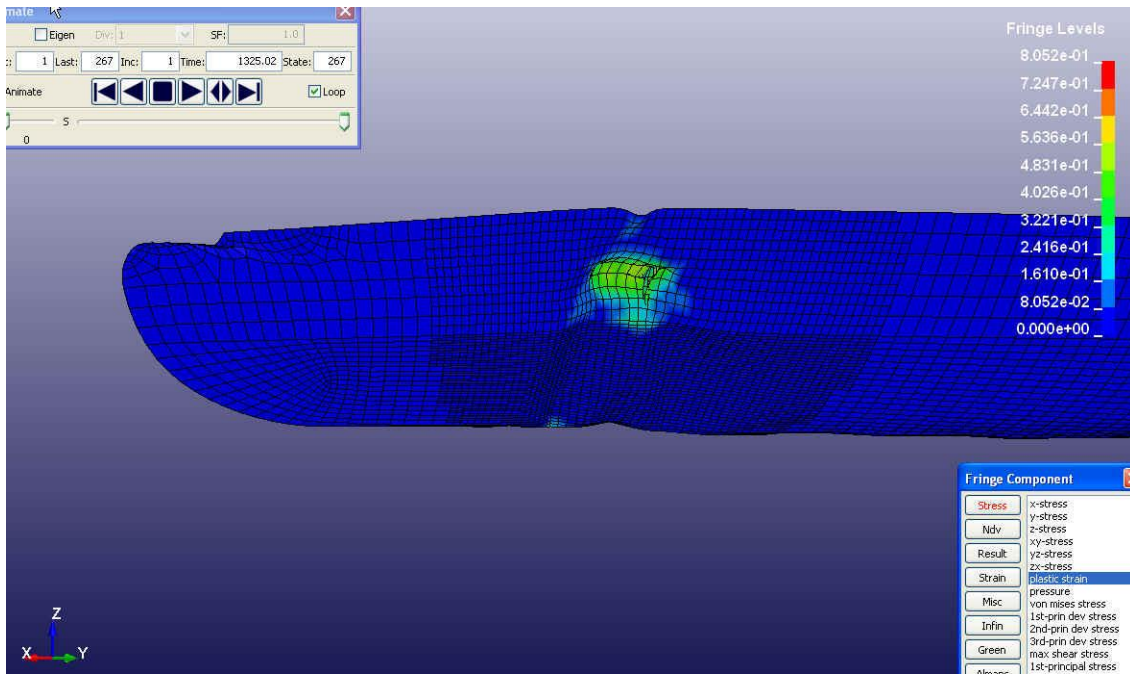
Figure 23 – PC1-2 XFEM – Plastic Strain
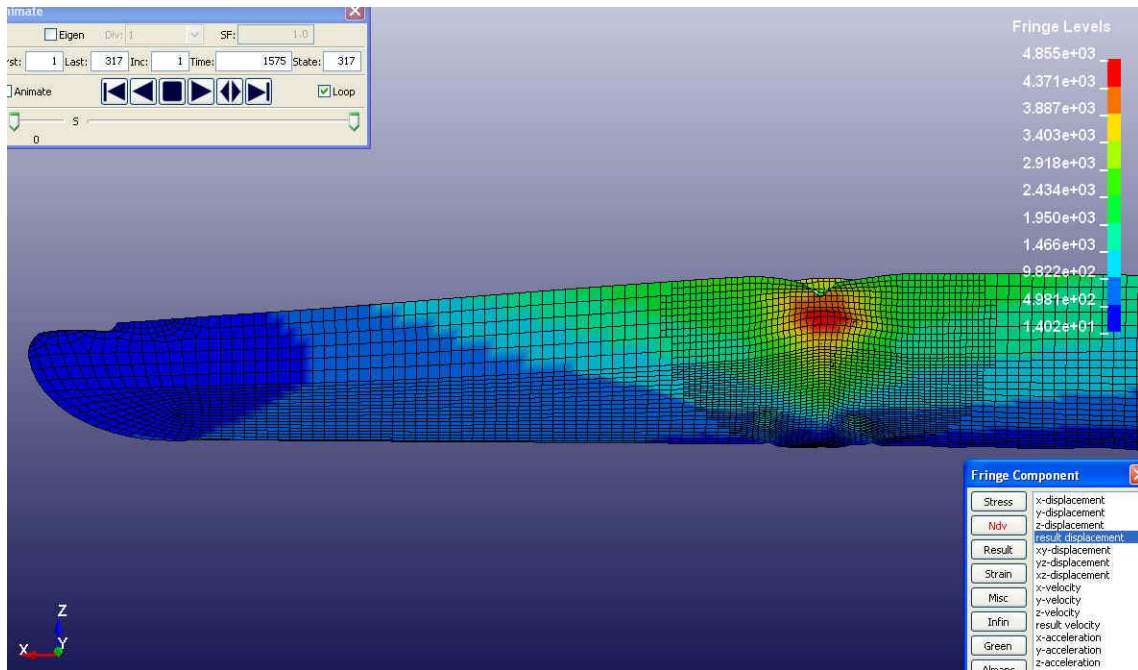
Figure 24 – PC1-4 FEM – Total Displacement
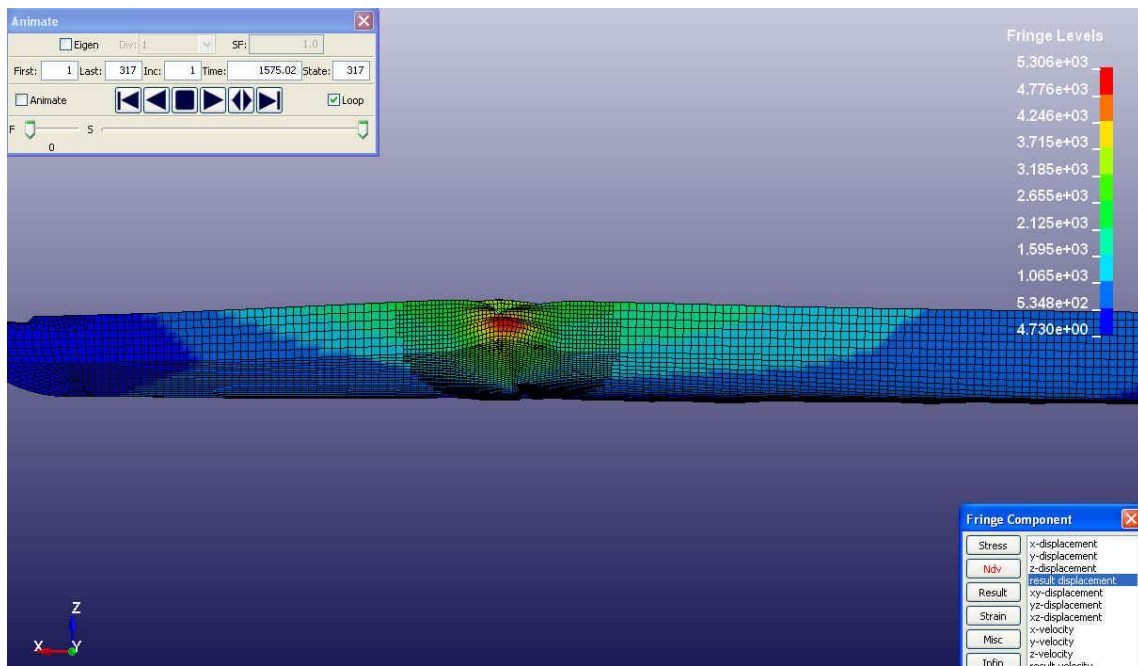
Figure 25 – PC1-4 XFEM – Total Displacement

38
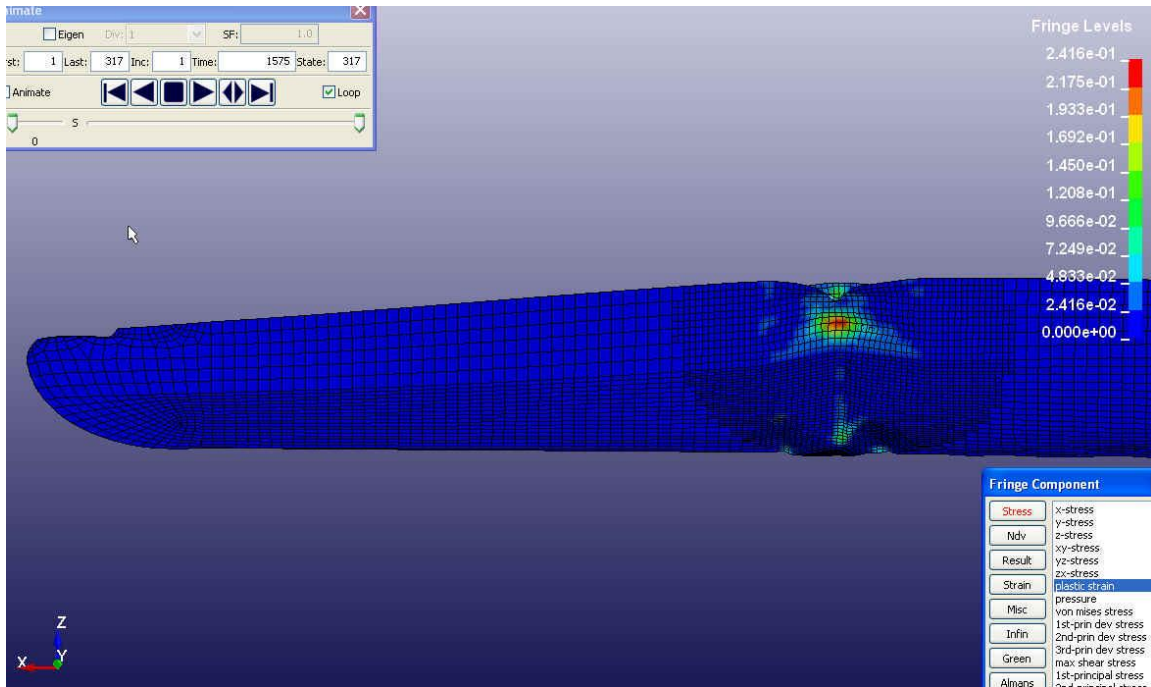
Figure 26 – PC1-4 FEM – Plastic Strain
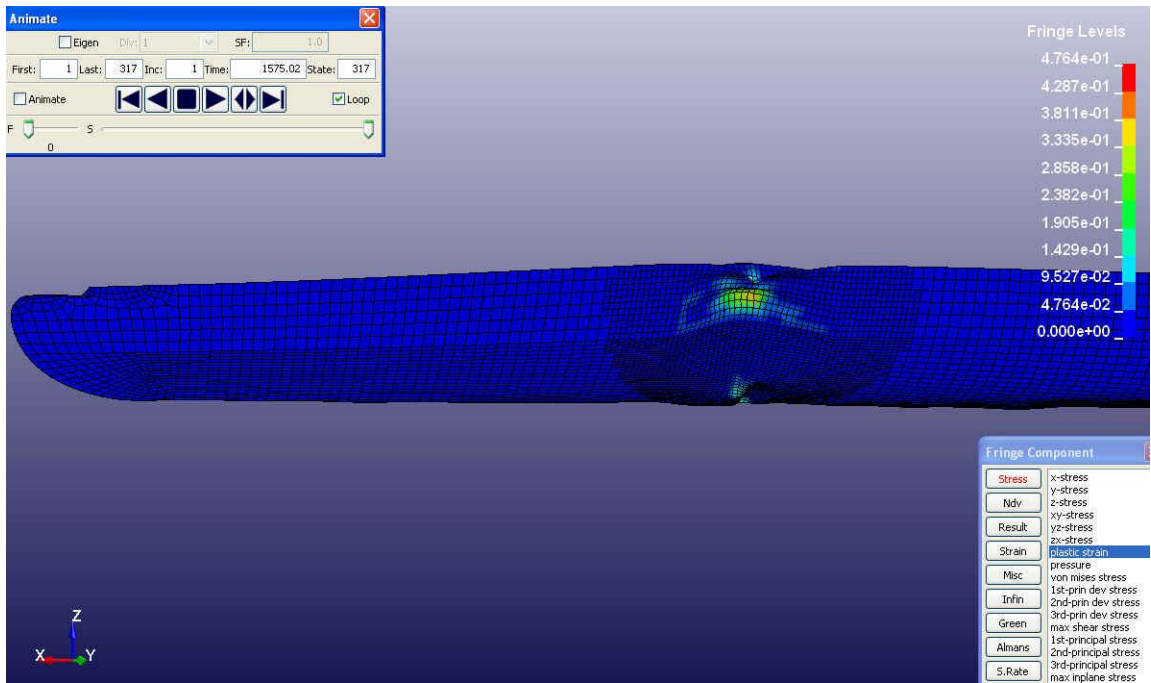
Figure 27 – PC1-4 XFEM – Plastic Strain

This page intentionally left blank

References

1- T. Belytschko, Y.Krongaus, D. Organ, M.Fleming, P. Krysl, Meshless Methods: An Overview and Recent Developments, Computer Methods in Applied Mechanics and Engineering, 139: 3-47, 1996
2- S. Li, W.K. Liu, Meshfree and particle methods and their applications, Applied Mechanics Review, 55, no. 5, 2002
3- J.A.T. Freitas. Hybrid-Trefftz displacement and stress elements for elastodynamic analysis in the frequency domain, Computer Assisted Mechanics and Engineering Sciences, 4: 345-368, 1997
4- Corneliu Cismasiu. The Hybrid-Trefftz Displacement Element for Static and Dynamic Structural Analysis Problems, Doctoral thesis, Universidade Técnica de Lisboa, 2000
5- Tomasz Klekiel, J. A. Kolodziej, Trefftz method for large deflection of plates with application of evolutionary algorithms, Computer Assisted Mechanics and Engineering Sciences, 13: 407-416, 2006
6- Zi-Cai Li, Tzon-Tzer Lu, Hsin-Yun Hu, The collocation Trefftz method for biharmonic equations with crack singularities, Engineering Analysis with Boundary Elements, 28: 79-96, 2004
7- Vladimir Kompis, Mario Stiavnicky, Trefftz functions in FEM, BEM and Meshless methods, Computer Assisted Mechanics and Engineering Sciences, 13: 417-426, 2006
8- P. Krysl, T. Belytschko, The Element Free Galerkin Method for Dynamic Propagation of Arbitrary 3-D cracks, International Journal for Numerical Methods in Engineering, 44: 767-800, 1999
9- C.A. Duarte, J. Tinsley Oden, An h-p adaptive method using clouds, Computer Methods in Applied Mechanics and Engineering, 139:237-262, 1996
10- T. Most, C. Bucher, A Moving Least Squares weighing function for the Element-free Galerkin Method which almost fulfills essential boundary conditions, Structural Engineering and mechanics, 21: 315-332, (2005)
11- T. Belytschko, Y.Y. Lu, L. Gu, Element-Free Galerkin Methods, International Journal for Numerical Methods in Engineering, 37:229-256, 1994
12- B. Muravin, The Application of Element Free galerkinMethod in the Investigation of Crack Interaction, Doctoral thesis, Tel-Aviv University, 2003
13- C.A. Duarte, J. Tinsley Oden, H-p Clouds – An h-p Meshless Method, Numerical Methods for Partial Differential Equations, 12: 673-705, 1996
14- T. Menouillard, T. Belytschko, J-H Song, Smoothly discontinuous enrichment in XFEM fro dynamic crack propagation, IV European Conference on Computational Mechanics, Paris, France, ECCM 2010
15- N. Sukumar, J. Dolbow, A. Devan, J. Yvonnet, F. Chinesta, D. Ryckelynck, P. Lorong, I. Alfaro, M.A. Martinez, E. Cueto, M. Doblaré, Meshless Methods and Partition of Unity Finite Elements, International Journal of Forming Processes, 8: 409-427, 2005

16- J.M. Melenk, L. Babuska, The Partition of Unity Finite Element Method: Basic Theory and Applications, Seminar für Angewandte Mathematik Eidgenössische Technische Hochschule, Zürich, Switzerland, Resear Report No 96-01, 1996

17- N. Sukumar, J.H. Prévost, Modeling Quasi-static Crack Growth with the Extended Finite Element Method. Part I: Computer Implementation, International Journal of Solids and Structures, 2003

18- J. Dolbow, N. Moës, T. Belytschko, A Finite Element Method for Crack Growth Without Remeshing, International Journal for Numerical Methods in Engineering, 46: 131-150, 1999

19- S. Jiang, Z. Ying, C. Du, The Optimal XFEM approximation for fracture analysis, IOP Conf. Seires: Material Science and Engineering, vol 10, 2010

20- N. Moës, N. Sukumar, B. Moran, T. Belytschko, An Extended Finite Element Method (X-FEM) for Two and Three- Dimensional Crack Modeling, European Congress on Computational Methods in Applied Sciences and Engineering, ECCOMAS 2000

21- A. Ahmed, eXtended Finite Element Method 9XFEM)- Modeling arbitrary discontinuities and Failure analysis, Masters thesis, Istituto Universitario di Studi Superiori di Pavia, 2009

22- G. Zi, T. Belytschko, New crack-tip elements for XFEM and applications to cohesive cracks, International Journal for Numerical Methods in Engineering, 57: 2221-2240, 2003

23- Osher,S. J.; Fedkiw, R.P., "Level Set Methods and Dynamic Implicit Surfaces, Springer-Verlag, 2002

24- Claude Daley, "Direct Design for Polar Ships (DDPS), developed from the IACS UR for Polar Ships", 2010

25- Daley C., Jiancheng L., "Assessment of Ship Ice Loads in Pack Ice", Icetech10, 2010.

26- "Requirements concerning POLAR CLASS", Report UR -1, International Association of Classification Societies, 2001

27- Claude Daley, "Energy Based Ice Collision Forces", Porc. Of the 15th International Conference on Port and Ocean Engineering under Artic Conditions" Helsinki University of Technology, Finland, August 1999.

Appendix A

Figures A1 through A20 are plots of the Transient Ice Loads on the hull plating during collision. These loads are calculated using the DDPS algorithm.
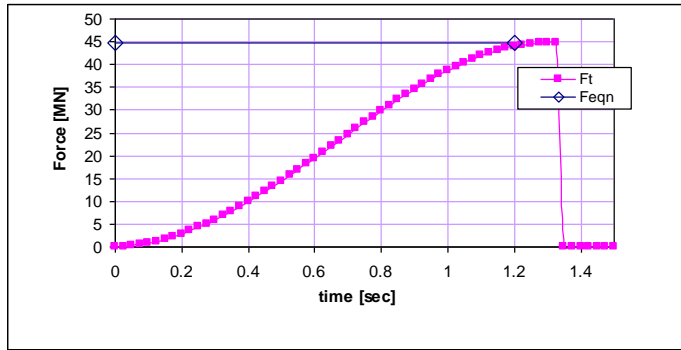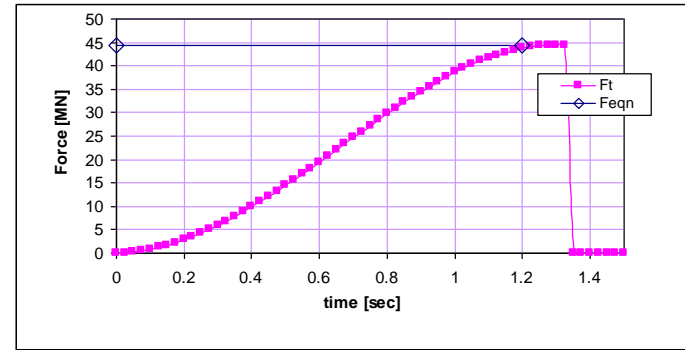

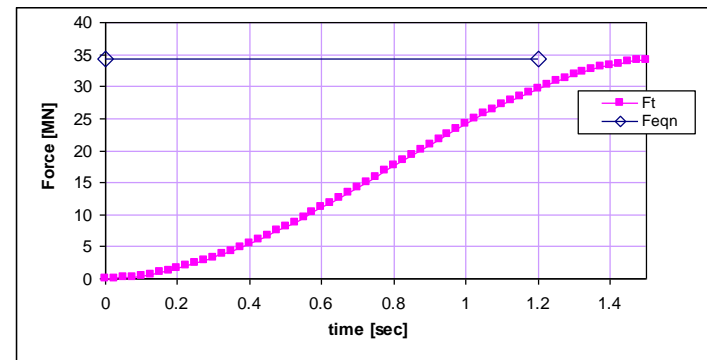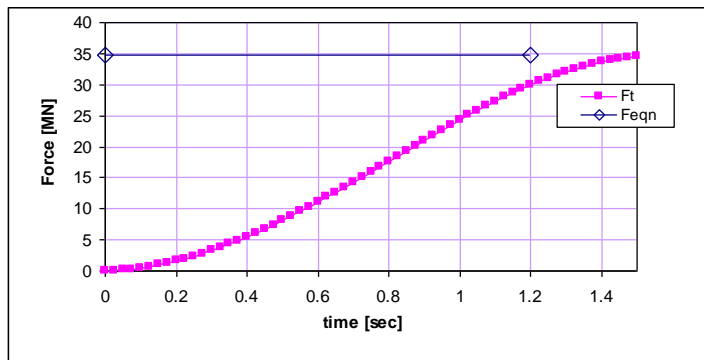Figure A1 - PC1_1 Ice load

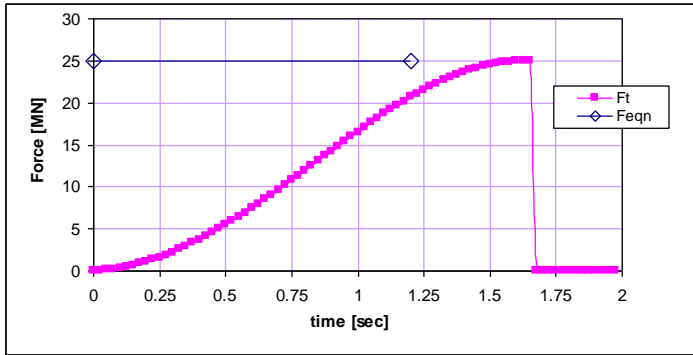Figure A2 - PC1_2 Ice Load

Figure A3 - PC1_3 Ice Load

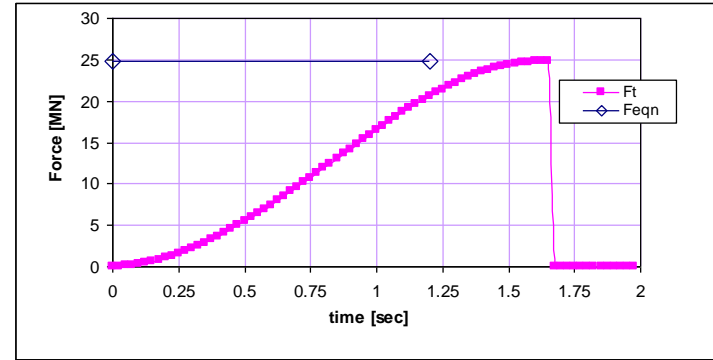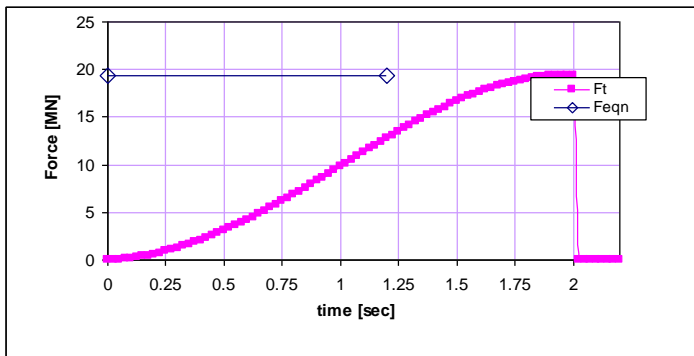Figure A4 - PC1_4 Ice Load

Figure A5 - PC2_1 Ice Load

Figure A6 - PC2_2 Ice Load
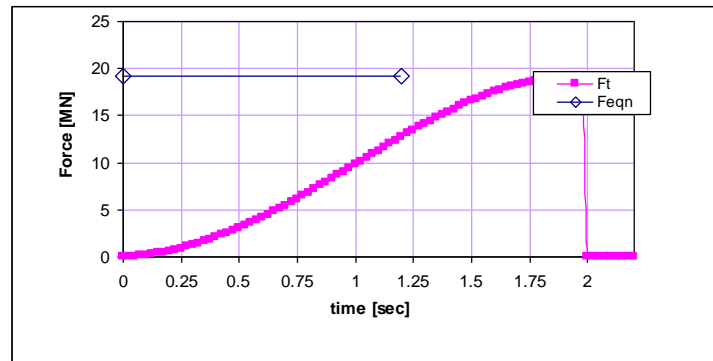
Figure A7 - PC2_3 Ice Load
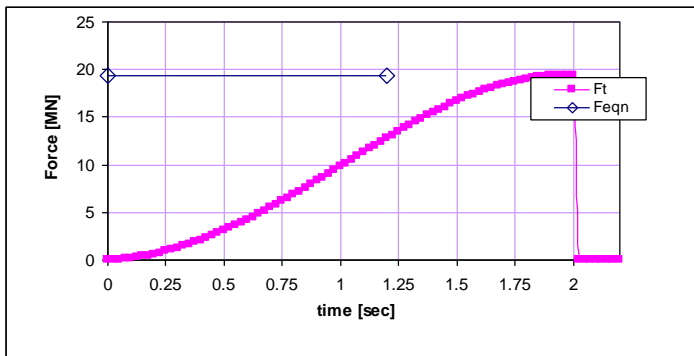
Figure A8 - PC2_4 Ice Load

Figure A9 - PC3_1 Ice Load

Figure A10 - PC3_2 Ice Load
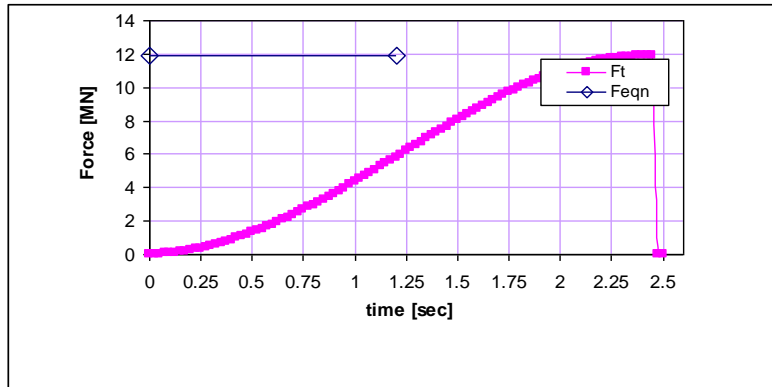
Figure A11 - PC3_3 Ice Load
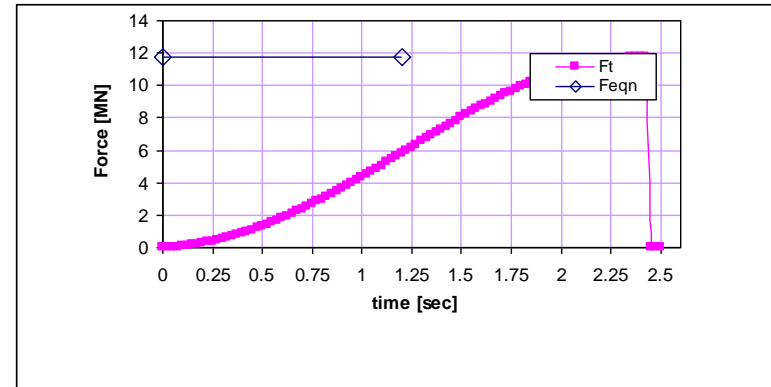
Figure A12 - PC3_4 Ice Load
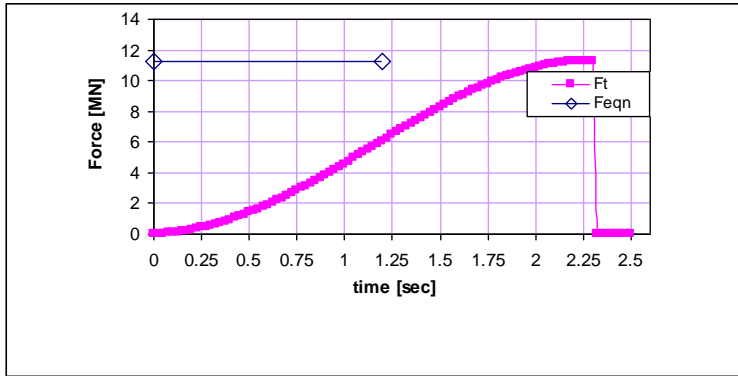
Figure A13 - PC4_1 Ice Load
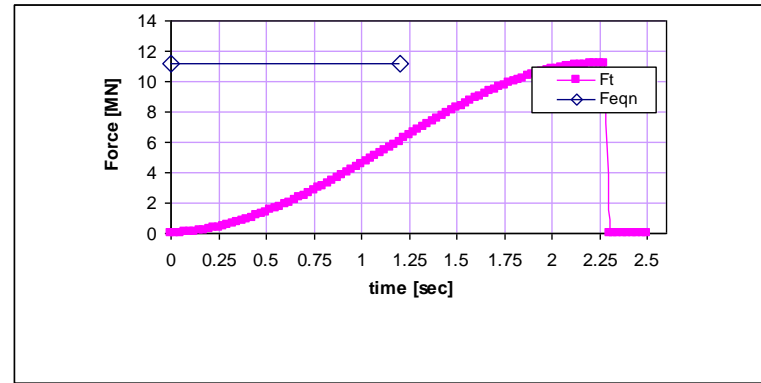
Figure A14 - PC4_2 Ice Load
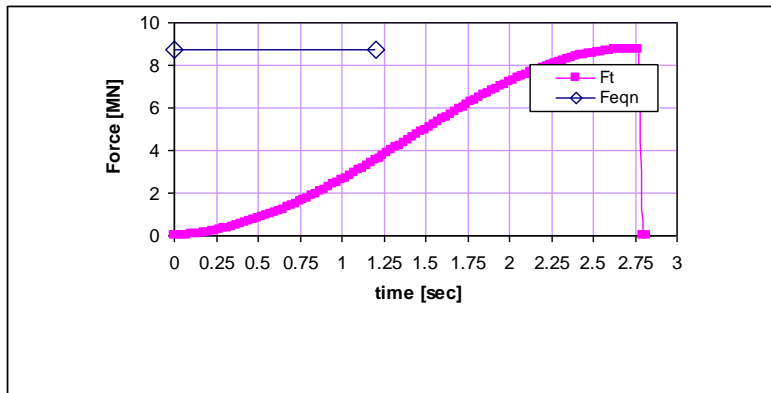
Figure A15 - PC4_3 Ice Load
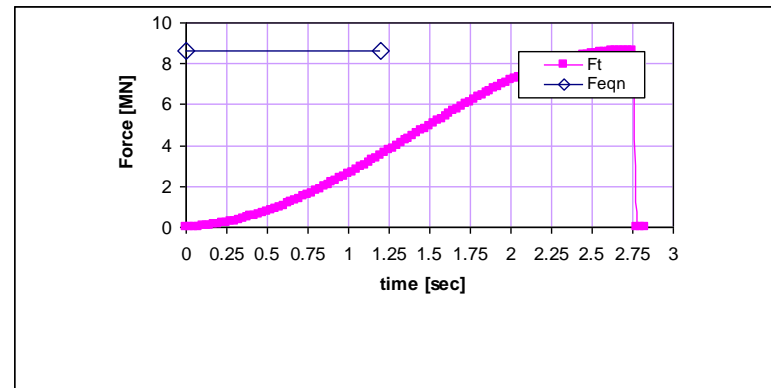
Figure A16 - PC4_4 Ice Load
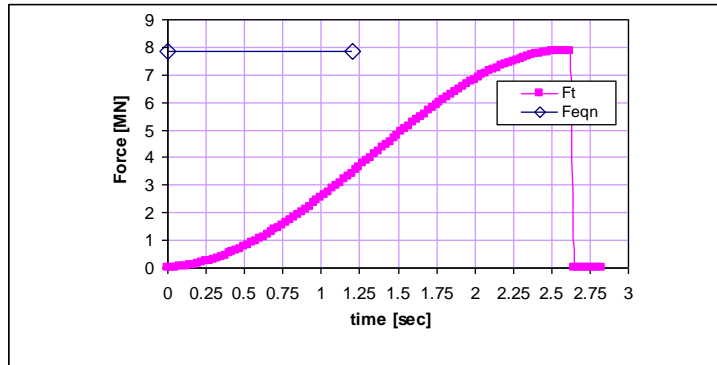
Figure A17 - PC5_1 Ice Load

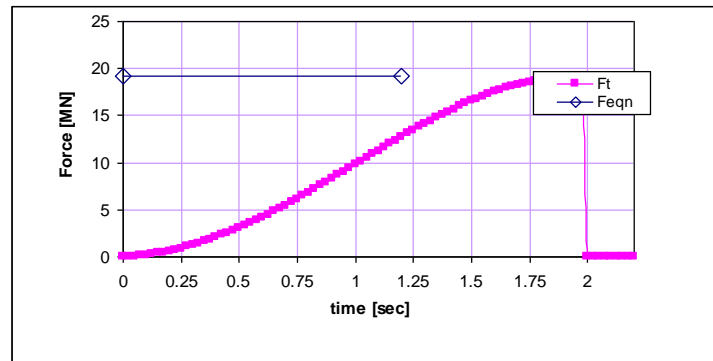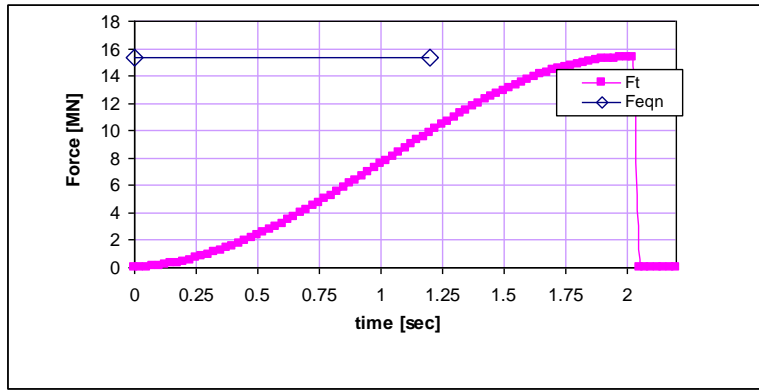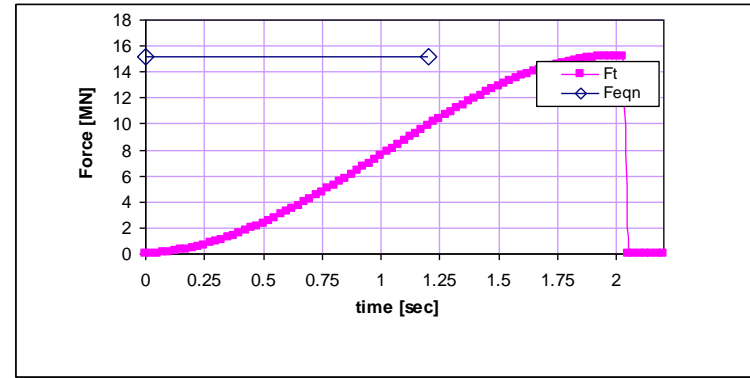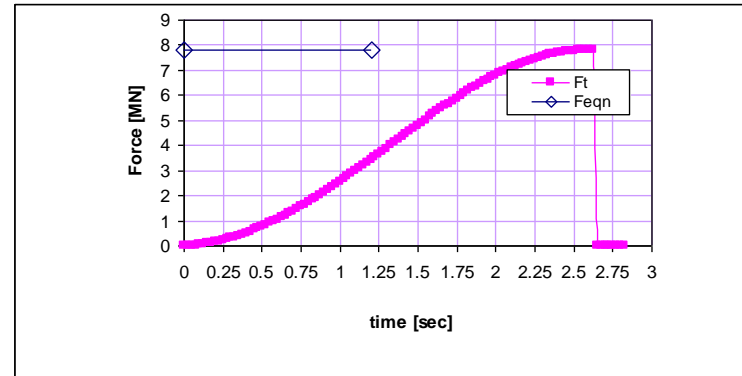Figure A18 - PC5_2 Ice Load
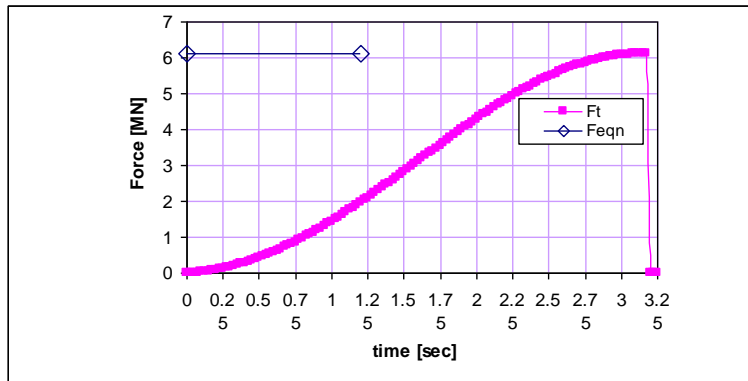
Figure A19 - PC5_3 Ice Load
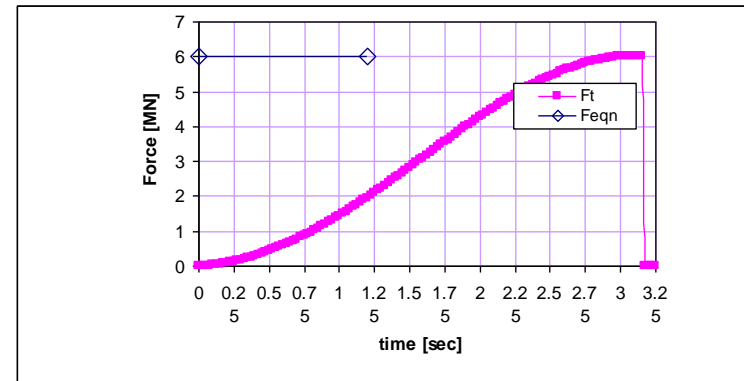
Figure A20 - PC5_4 Ice Load

47

This page intentionally left blank

Appendix B

Algorithm for a Pre-processor for generating the input file to model the impact of Sea Ice on the Ship hull structure using LS-DYNA

The purpose of the development of this pre-processor is based on the requirement for creating a framework on which to conduct reliably and expediently further research on the study of crack initiation and propagation on any specified hull form. This tool will facilitate the process of generating the required model definition as input to the LS-DYNA solver.

A basic flowchart of the primary components of the algorithm developed is described first. The actual code, written in Fortran, follows.

This page intentionally left blank

Sea Ice Impact on Hull Structures - Pre processor for Generation of Input to LS-DYNA

Read Input Data

Read: Hull form, Principals, Locations of Decks, Bulkheads, Sea Ice Impact information, Method for modeling Crack Propagation

Generate Initial Hull Mesh

From Hull form

Calculate location and Area of Ice Impact on the Hull

Method of Modeling Crack Initiation and Propagation

FEM

EFGM

X-FEM

Mesh Refinement in area of impact for FEM type elements

Mesh Refinement in area of impact foe X-FEM type elements

Mesh Refinement in area of impact for Element Free Galerkin type elements

A

(continued)

A

Follows IACS UR Rules for Polar Ships

Calculate Ice Load History on Hull

Generate Mesh for Decks - Include refinement in the Impact zone

Generate Mesh for Transverse Bulkheads - Include refinement in the Impac zone

Determine positions of Stanchions and generate

Generate All Elements

From required total Displacement, calculate cross-sections of Stanchions

Write output file in LS-DYNA format for direct input to Executable process

End

PROJECT TECHNICAL COMMITTEE MEMBERS

The following persons were members of the committee that represented the Ship Structure Committee to the Contractor as resident subject matter experts. As such they advised the contractor in cognizant matters pertaining to the contract of which the agencies were aware, performed technical review of the work in progress and edited the final report.

Chairman	**Mr. Timothy McAllister**	**USCG**
Contracting Officer's Technical Representative:		
Executive Director Ship Structure Committee:	**LCDR Ronald Caputo**	**USCG**
Members:	**Li Lin**	**ABS**
	Roger Basu	**ABS**
	Yoo Sang Choo	
	Jeom Paik	**Nat'l University of Pusan**
	David Manning	**Tidewater**
	Robert Dow	**Newcastle University**
	Pramod Dash	**Hindustan Institute of Technology**
	Malcolm Smith	**DRDC**
	Paul Franklin	**Bath Iron Works**
	Fai Cheng	**Lloyd's Register**
	Robert Tustin	**Lloyd's Register**
	Han-Chang Yu	**ABS**
	Alfred Tunik	**Consultant**

SHIP STRUCTURE COMMITTEE LIAISON MEMBERS

LIAISON MEMBERS

American Society of Naval Engineers	Captain Dennis K. Kruse (USN Ret.)
Bath Iron Works	Mr. Steve Tarpy
Colorado School of Mines	Dr. Stephen Liu
Edison Welding Institute	Mr. Rich Green
International Maritime Organization	Mr. Igor Ponomarev
Int'l Ship and Offshore Structure Congress	Dr. Alaa Mansour
INTERTANKO	Mr. Dragos Rauta
Massachusetts Institute of Technology	
Memorial University of Newfoundland	Dr. M. R. Haddara
National Cargo Bureau	Captain Jim McNamara
National Transportation Safety Board - OMS	Dr. Jack Spencer
Office of Naval Research	Dr. Yapa Rajapaksie
Oil Companies International Maritime Forum	Mr. Phillip Murphy
Samsung Heavy Industries, Inc.	Dr. Satish Kumar
United States Coast Guard Academy	Commander Kurt Colella
United States Merchant Marine Academy	William Caliendo / Peter Web
United States Naval Academy	Dr. Ramswar Bhattacharyya
University of British Columbia	Dr. S. Calisal
University of California Berkeley	Dr. Robert Bea
Univ. of Houston - Composites Eng & Appl.	
University of Maryland	Dr. Bilal Ayyub
University of Michigan	Dr. Michael Bernitsas
Virginia Polytechnic and State Institute	Dr. Alan Brown
Webb Institute	Prof. Roger Compton

RECENT SHIP STRUCTURE COMMITTEE PUBLICATIONS

Ship Structure Committee Publications on the Web - All reports from SSC 1 to current are available to be downloaded from the Ship Structure Committee Web Site at URL:
http://www.shipstructure.org
SSC 445 – SSC 393 are available on the SSC CD-ROM Library. Visit the National Technical Information Service (NTIS) Web Site for ordering hard copies of all SSC research reports at URL: http://www.ntis.gov

SSC Report Number	Report Bibliography
SSC 464	Design and Detailing for High Speed Aluminum Vessels Design Guide and Training Mish, Wh Jr., Lynch T., Hesse E., Kulis J., Wilde J., Snyder Z., Ruiz F. 2012
SSC 463	Marine Composites NDE, Inspection Techniques for Marine Composite Construction Greene, E 2012
SSC 462	Review of Current Practices of Fracture Repair Procedures for Ship Structures Wang, G, Khoo, E., ABS Corporate Technology 2012
SSC 461	Structural Challenges Faced By Arctic Ships, Kendrick A., Daley C. 2011
SSC 460	Effect of Welded Properties on Aluminum Structures, Sensharma P., Collette M., Harrington J. 2011
SSC 459	Reliability-Based Performance Assessment of Damaged Ships, Sun F., Pu Y., Chan H., Dow R.S., Shahid M., Das P.K. 2011
SSC 458	Exact Mapping of Residual Stress in Ship Hull Structures by Use of Neutron Diffraction Das. S. Kenno S. 2009
SSC 457	Investigation of Plastic Limit States for Design of Ship Hull Structures, Daley C., Hermanski G. 2009
SSC 456	Buckling Collapse Testing on Friction Stir Welded Aluminum Stiffened Plate Structures, Paik J.K. 2009
SSC 455	Feasibility, Conceptual Design and Optimization of a Large Composite Hybrid Hull, Braun D., Pejcic M. 2008
SSC 454	Ultimate Strength and Optimization of Aluminum Extrusions, Collette M., Wang C. 2008
SSC 453	Welding Distortion Analysis Of Hull Blocks Using Equivalent Load Method Based On Inherent Strain, Jang C.D. 2008
SSC 452	Aluminum Structure Design and Fabrication Guide, Sielski R.A. 2007
SSC 451	Mechanical Collapse Testing on Aluminum Stiffened Panels for Marine Applications, Paik J.K. 2007